European Journal of Medicinal Chemistry 272 (2024) 116487

Contents lists available at ScienceDirect

European Journal of Medicinal Chemistry

journal homepage: www.elsevier.com/locate/ejmech

Research paper

Design, synthesis and bioactivity evaluation of 4-hydroxycoumarin derivatives as potential anti-inflammatory agents against acute lung injury and colitis

Xiaobo Li [a,b,d], Xinyi Huang [c], Yunxi Zhao [b,d], Zhiwei Zheng [b,d], Mi Guo [b,d], Zhicao Chen [b,d], Pan Chen [b,d], Xiang Li [b,d], Jing Liao [b,d], Miao Jiang [b,e], Won-Jea Cho [f], Young-Chang Cho [f], Ruifeng Zeng [e,**], Qidong Tang [b,d,*], Guang Liang [a,b,d,***]

[a] Department of Pharmacy and Institute of Inflammation, Zhejiang Provincial Peoples Hospital, Affiliated Peoples Hospital, Hangzhou Medical College, Hangzhou, 310014, China
[b] Wenzhou Institute, University of Chinese Academy of Sciences, Wenzhou, 325001, China
[c] Department of Nursing, The First Affiliated Hospital of Wenzhou Medical University, Wenzhou, 325035, China
[d] Chemical Biology Research Center, School of Pharmaceutical Sciences, Wenzhou Medical University, Wenzhou, 325035, China
[e] Department of Anesthesiology and Perioperative Medicine, The Second Affiliated Hospital and Yuying Children's Hospital of Wenzhou Medical University, Key Laboratory of Anesthesiology of Zhejiang Province, Wenzhou Medical University, Wenzhou, 325035, China
[f] College of Pharmacy, Chonnam National University, Gwangju, 61186, South Korea

ARTICLE INFO

Keywords:
4-Hydroxycoumarin derivatives
Acute lung injury
Colitis
Anti-inflammatory
MAPK
IRAK1

ABSTRACT

Acute lung injury (ALI) and inflammatory bowel disease (IBD) are common inflammatory illnesses that seriously affect people's health. Herein, a series of 4-hydroxylcoumarin (4-HC) derivatives were designed and synthesized. The inhibitory effects of these compounds on LPS-induced interleukin-6 (IL-6) release from J774A.1 cells were then screened via ELISA assay, compound **B8** showed 3 times more active than the lead compound 4-HC. The most active compound **B8** had the IC_{50} values of 4.57 μM and 6.51 μM for IL-6 release on mouse cells J774A.1 and human cells THP-1, respectively. Furthermore, we also found that **B8** could act on the MAPK pathway. Based on the target prediction results of computer virtual docking, kinase inhibitory assay was carried out, and it revealed that targeting IRAK1 was a key mechanism for **B8** to exert anti-inflammatory activity. Moreover, **B8** exerted a good therapeutic effect on the dextran sulfate sodium (DSS)-induced colitis model and liposaccharide (LPS)-induced ALI mouse models. The acute toxicity experiments indicated that high-dose **B8** caused no adverse reactions in mice, confirming its safety *in vivo*. Additionally, the preliminary pharmacokinetic (PK) parameters of **B8** in SD rats were also examined, revealing a bioavailability (F) of 28.72 %. In conclusion, **B8** is a potential candidate of drug for the treatment of ALI and colitis.

1. Introduction

Inflammation is a physiological process initiated when organisms respond to harmful stimuli such as pathogens, viruses, and foreign particles [1,2]. The inflammatory pathway comprises inducers, sensors, mediators and target tissues. Inducers (such as lipopolysaccharides (LPS)) trigger an inflammatory response and can be detected by the sensors [3]. On the other hand, sensors such as TLRs are activated on specific cells, including tissue-resident macrophages [4], dendritic cells (DCs), and mast cells [5]. Sensors stimulate the production of mediators, such as cytokines [6], chemokines [7], arachidonic acids [8], and proteolytic cascades (including bradykinins) [9]. Inflammatory mediators target different tissues, leading to alterations in their functional status. Inflammation plays a pivotal role in the advancement of numerous conditions, such as acute lung injury (ALI) and inflammatory bowel disease (IBD) [10,11]. Both of these illnesses involve the production of

* Corresponding author. Wenzhou Institute, University of Chinese Academy of Sciences, Wenzhou, 325001, China.
** Corresponding author.
*** Corresponding author. Department of Pharmacy and Institute of Inflammation, Zhejiang Provincial Peoples Hospital, Affiliated Peoples Hospital, Hangzhou Medical College, Hangzhou 310014, China.
E-mail addresses: ruifengzeng@163.com (R. Zeng), tangqidongcn@126.com (Q. Tang), wzmcliangguang@163.com (G. Liang).

https://doi.org/10.1016/j.ejmech.2024.116487
Received 22 February 2024; Received in revised form 1 May 2024; Accepted 5 May 2024
Available online 10 May 2024

pro-inflammatory factors such as interleukin-6 (IL-6), leading to tissue damage and various symptoms [12,13].

Injury to alveolar epithelial cells and capillary endothelial cells induced by various direct and indirect factors is a major cause of ALI. The disease is often characterized by diffuse pulmonary interstitial and alveolar edema, ultimately leading to acute hypoxic respiratory insufficiency [14]. Bacterial or viral infections can also cause ALI, such as pneumonia resulting from the recently widely publicized novel coronavirus [15,16]. On the other hand, Crohn's disease and ulcerative colitis (UC) are some of the examples of IBD. UC mainly involves the colon and rectum [17]. In the disease, the range of lesions is generally limited to the intestinal mucosal layer, which is characterized by continuous mucosal inflammation, often accompanied by diarrhea, hematochezia, abdominal pain and other symptoms. While UC could easily progress to colon cancer, its exact cause is very complex and remains elusive [18]. In clinical practice, the management of ALI focuses on inflammation control through corticosteroids. The treatment of UC typically involves corticosteroids or non-steroidal anti-inflammatory drugs (5-ASA) to manage inflammation and enhance quality of life, thereby alleviating the disease [19]. Since steroid or non-steroidal anti-inflammatory drugs still have many limitations in clinical practice, developing new drugs for controlling ALI and UC is imperative.

Many marketed drugs are derived from natural products, such as Galanthamine, Calanolide A, Arteether, Warfarin, and Methoxsalen as shown in Fig. 1, which were discovered by retaining the active skeleton of natural products and then making corresponding modification to enhance their biological activity and drug-likeness. Galanthamine has been used to treat neurodegenerative diseases [20]. Arteether is widely used in malaria treatment [21]. Calanolide Ais is used as an anti-HIV drug [22]. Our research group has been engaged in the modification on the natural products for more than a decade, such as the work of cinnamamide derivatives **2i** and **L26** published on *J. Med. Chem.* [23] and *Eur. J. Med. Chem.* [24], respectively, as illustrated in Fig. 1. Coumarin exhibits a broad spectrum of pharmacological activities including anti-HIV [25], anti-tumor [26], anti-hypertension [27], anti-hyperlipidemia [28], anti-inflammatory [29] and analgesic effects [30]. Many coumarin-based medications, such as Methoxsalen and Warfarin, are already on the market. Moreover, both coumarin and 4-Hydroxycoumarin (4-HC) have demonstrated anti-inflammatory activity in TNBS-induced colitis in rat models [31]. Additionally, C-4-modified coumarin compounds exhibited potent anti-inflammatory and analgesic activities, as well as a positive regulation and inhibition of inflammatory factors [32]. Therefore, synthesizing new derivatives with improved pharmacological or pharmacokinetic (PK) properties by chemically modifying the 4-HC framework is crucial for drug research and development.

In this study, we used 4-HC as the lead compound to make modification by retaining the dominant fragment of coumarin skeleton. The primary objective of the modification is to introduce flexible hydrophilic or lipophilic segments at the 4-hydroxyl position. The structure of enrofloxacin, an anti-inflammatory drug, contains a hydrophilic piperazine ring (Fig. 2). Some commercially available or to-be-marketed drugs, such as Ensaculin and Morniflumate, also have hydrophilic piperazine rings and morpholine rings. Inspired by this, hydrophilic fragments with similar structures, such as ethylpiperazine and acetylpiperazine, were introduced. Furthermore, benzene ring and thiophene ring are common in the structure of drugs, such as cephalothin sodium, phenylbutazone, ensaculin, and morniflumate. Additionally, fat-soluble groups like benzene and thiophene rings were introduced to investigate their impact on biological activity. Therefore, we modified 4-HC from the two dimensions by introducing fat solubility or water solubility fragments to design the target compounds.

Herein, 25 4-HC derivatives were successfully synthesized, in which 15 compounds showed better inhibition effect than 4-HC on the LPS-induced IL-6 release from J774A.1 mouse cells in ELISA assay. Compound **B8** showed 3 times more active than the lead compound 4-HC and exhibited a concentration gradient inhibition with the IC_{50} of 4.57 μM and 6.51 μM for IL-6 release on mouse cells J774A.1 and human cells THP-1 cells, respectively. Furthermore, **B8** demonstrated minimal cytotoxicity and animal toxicity, affirming its safety profile. Overall, our investigations, both *in vitro* and *in vivo*, suggest that **B8** holds promise as a prospective therapeutic agent for addressing LPS-induced ALI and DSS-induced colitis.

2. Results and discussion

2.1. Chemistry

This paper describes two synthetic schemes for producing the 25 derivatives of 4-HC. Scheme 1 illustrates the synthesis process of compounds **A1-A8**, in which 4-HC and potassium carbonate (K_2CO_3) were combined with *N,N*-dimethyldiamine (DMF). Subsequently, halogenated benzene fragments, halogenated nitrogen fragments, halogenated morpholine fragments, halogenated piperazine fragments, or halogenated propylene oxide fragments were added. The resulting mixture underwent a reaction at 80 °C for 3 h, yielding compounds **A1-A8** through a nucleophilic substitution reaction.

Scheme 2 illustrates an alternative synthetic pathway for compounds **B1–B9** and **C1–C8.** Initially, 4-HC was dissolved in DMF followed by the addition of K_2CO_3. Subsequently, three equivalents of 1,2-

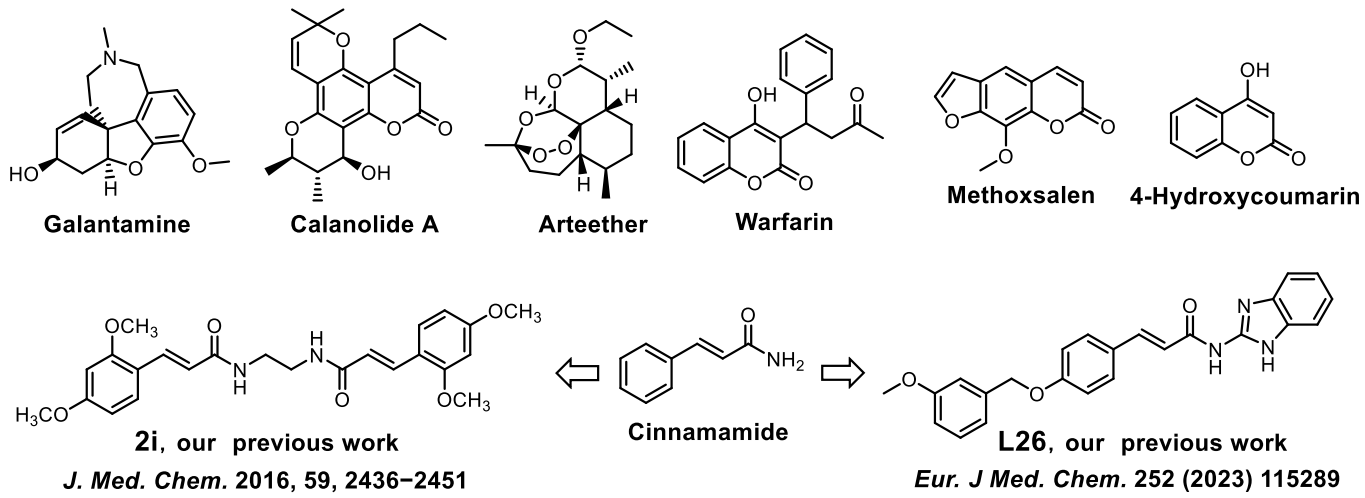

Fig. 1. Representative natural products and its derivatives.

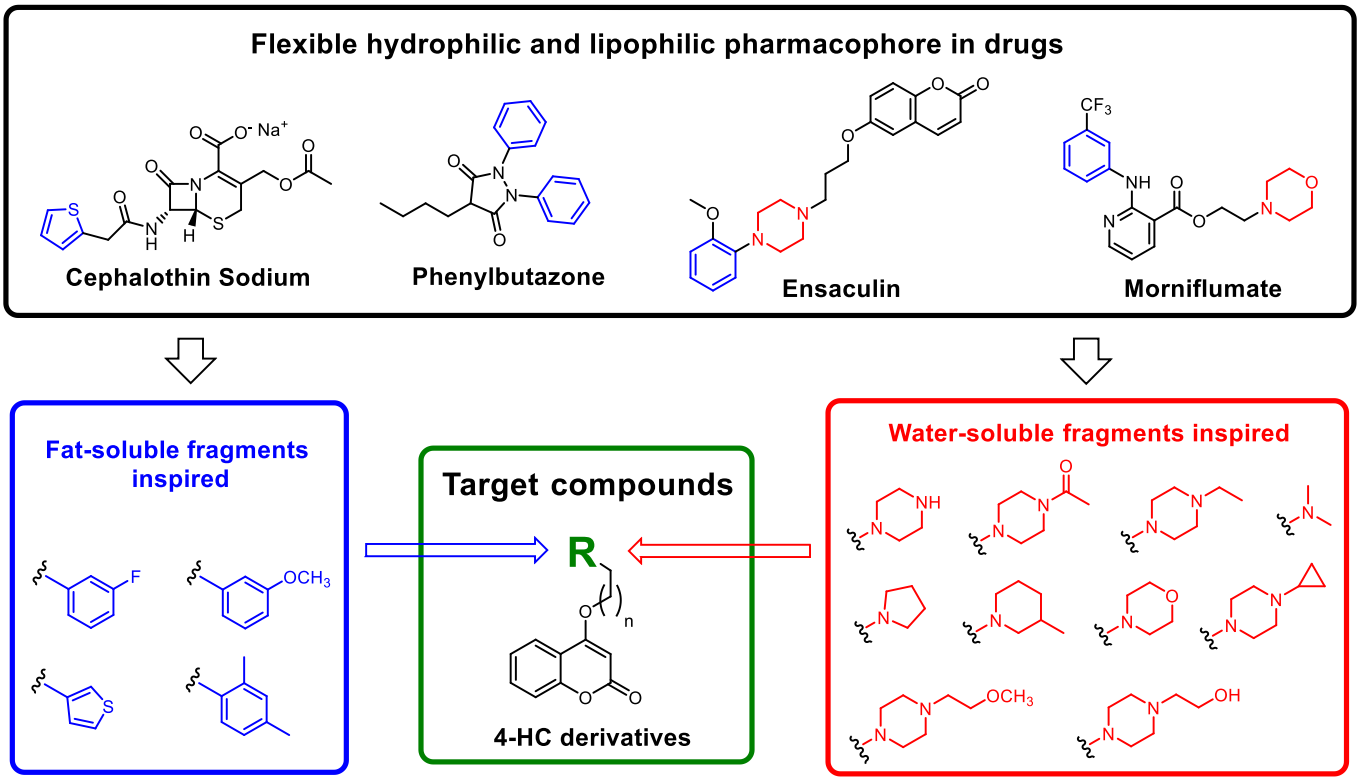

Fig. 2. Design and modification strategy for the 4-HC derivatives.

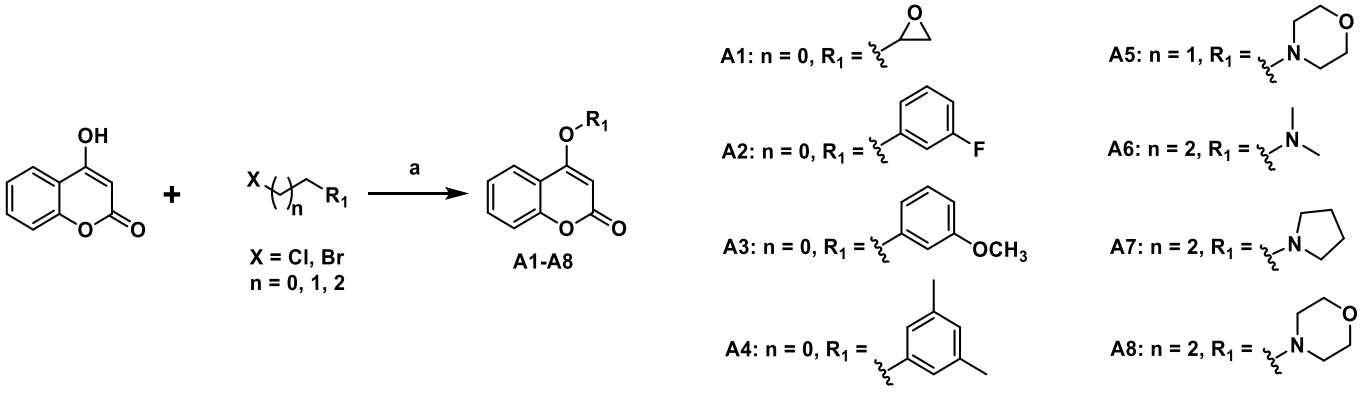

Scheme 1. Reagents and conditions: (a) K_2CO_3, halogenated hydrocarbons, DMF, 80 °C, 4 h.

dibromoethane and 1,3-dibromopropane were introduced to the mixture. The resulting reaction mixture was then refluxed at 80 °C for 3 h, yielding intermediates **a1** and **b1**. Subsequently, **a1** and **b1** were dissolved in DMF, and then K_2CO_3 was added to facilitate the reaction with piperazine, morpholine, and nitrogen heterocyclic rings. This reaction proceeded overnight at 80–90 °C, yielding compounds **B1–B9** and **C1–C8**.

Following the synthesis process, the synthesized compounds were purified using a chromatographic column to obtain a pure form of the final product. Subsequently, a detailed characterization and identification process was conducted utilizing a range of analytical techniques, such as NMR and LC-MS, enabling the determination of the chemical structure and molecular composition of the compounds.

Furthermore, to ensure the quality and purity of the compounds, HPLC analysis was performed. The results demonstrated that the purity of all compounds exceeded 95 %, indicating a high level of purity and confirming the success of the purification process. Overall, this paper provides a comprehensive and detailed account of the synthesis, purification, and characterization of 4-HC derivatives. The utilization of multiple analytical techniques enhances the reliability and accuracy of the findings.

2.2. Initial assessment of the 4-HC derivatives that inhibit the LPS-induced release of IL-6 and SAR analysis

Evaluating the potential anti-inflammatory activity of compounds *in vitro* by measuring the expression levels of inflammatory factors (such as IL-6) using the Enzyme-linked immunosorbent assay (ELISA) is a practical approach in this case [33]. Our group has accumulated experience in the study of inflammation for more than ten years, and the method of ELISA was used to test the preliminary anti-inflammatory activity of compounds at 10 μM in our published work in *Journal of Medicinal Chemistry* [34], *European Journal of Medicinal Chemistry* [35], *Nature Communications* [36], and so on. In this study, the anti-inflammatory

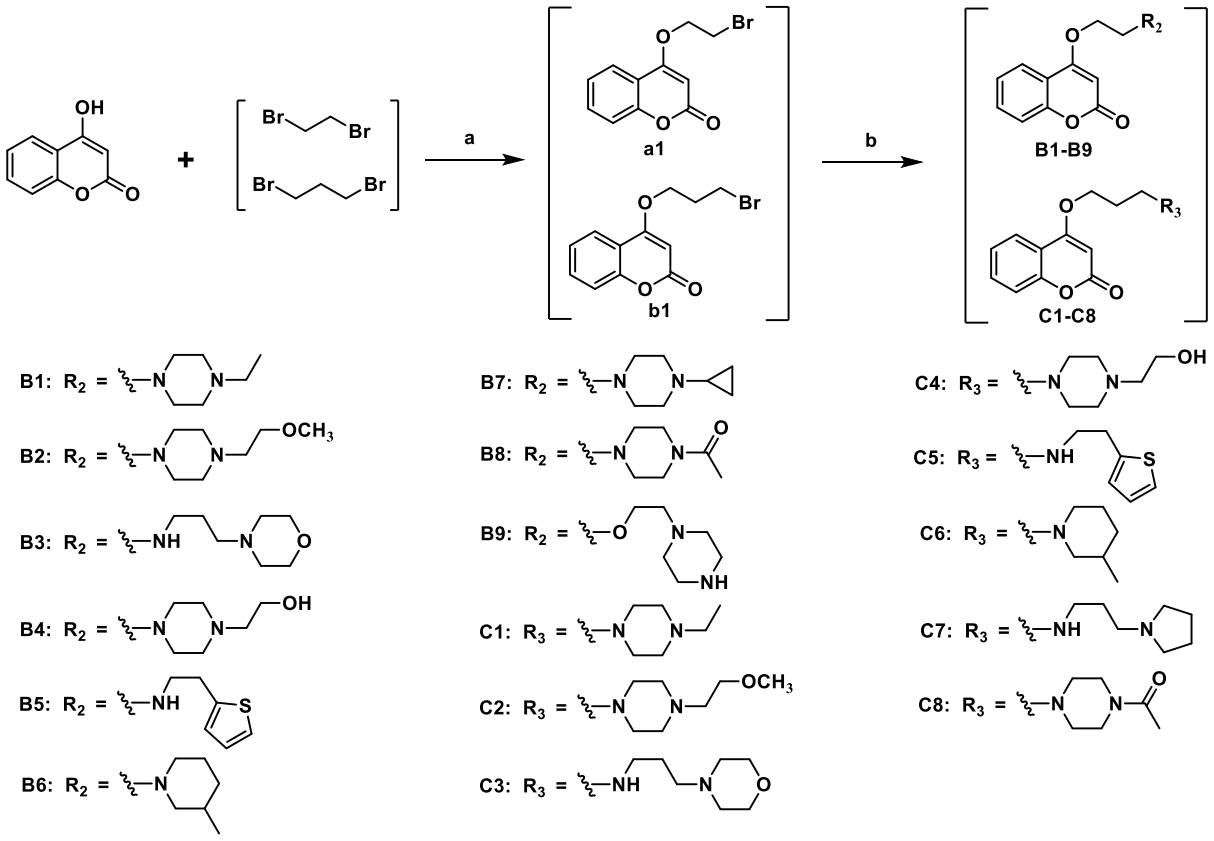

Scheme 2. Reagents and conditions: (a) K_2CO_3, DMF, 80 °C, 4 h. (b) K_2CO_3, piperazine derivatives, morpholine derivatives, morpholine derivatives, nitrogen heterocyclic ring, DMF, 80–90 °C, 4 h.

activity of 4-HC derivatives was also screened at 10 μM by ELISA to measure the IL-6 levels.

During this experiment, J774A.1 cells were treated with 10 μM 4-HC derivatives and 4-HC for 2 h before the addition of LPS. Following a 30-min incubation, the IL-6 levels in the medium were measured using an ELISA kit. The results, as shown in Table 1, indicate that a collective of 15 4-HC derivatives demonstrate superior efficacy in inhibiting LPS-induced IL-6 release compared to 4-HC. The most active compound **B8** showed 3 times more active than 4-HC. The experimental results revealed that when n = 0, except for compound **A3** (50.35 %), the introduction of water-soluble groups and fat-soluble groups did not obviously improve the biological activity. When n = 1, the introduction of some flexible hydrophilic fragments could significantly improve its anti-inflammatory activity, such as **B4** (48.76 %), **B6** (48.77 %), **B8** (51.59 %), and **B9** (50.08 %). The introduction of lipophilic fragments could only slightly improve the biological activity of **B5** (34.69 %). When n = 2, the introduction of some flexible hydrophilic fragments can improve its anti-inflammatory activity such as **C4** (51.26 %), **C7** (54.37 %), and **C8** (42.31 %). The introduction of lipophilic fragments loses activity, such as **C5**. Notably, the introduction of acetyl or hydroxyethyl groups on the piperazine ring significantly increased the activity of the derivatives when n = 1 or 2. Among the 25 4-HC derivatives, **A3**, **B8**, **B9**, **C4**, and **C7** exhibited the inhibition rates >50 % on IL-6. The increase in the carbon chain length with the same substituent sometimes enhances anti-inflammatory activity, while in other cases, it may diminish anti-inflammatory activity, with no specific pattern.

2.3. Cytotoxicity study of the 4-HC derivatives

Prior to a deeper investigation, we evaluated the viability of J774A.1 cells after exposure to the 4-HC derivatives at a concentration of 10 μM for 24 h. The survival rate was assessed using the Thiazolyl Blue (MTT) assay. According to the results, compounds **B8**, **B9**, **C4**, and **C8** exhibited non-toxic effects on J774A.1 cells (Fig. 3), indicating their relative safety. These findings provide initial evidence supporting these compounds' potential safety profile.

2.4. Dose-dependent inhibition of IL-6 release by compound *B8*

Compound **B8** was selected for gradient inhibition experiments after a thorough assessment of its biological activity and cytotoxicity based on established criteria J774A.1 cells were pretreated with various concentrations of **B8** for 30 min before being stimulated with 0.5 μg/mL of LPS to induce inflammation in triplicate experiments. Subsequently, IL-6 levels were then quantified using the established ELISA method. The inhibitory effect of **B8** on LPS-induced IL-6 production was dose-dependent, ranging from 2.5 μM to 10 μM (Fig. 4A and B). The IC_{50} values of **B8** against IL-6 release from mouse cells J774A.1 and human cells THP-1 were determined to be 4.57 μM and 6.51 μM, respectively. The dose-dependent inhibitory effect of **B8** on IL-6 release underscores its promise as a potent anti-inflammatory agent, warranting further investigation into its therapeutic potential.

2.5. Inhibition of the mRNA expression of compound *B8*

To investigate the mechanism of compound **B8** inhibiting the release of inflammatory cytokines, mRNA expression of IL-6 was determined at the gene transcription level using the real-time quantitative polymerase chain reaction (RT-qPCR). J774A.1 mouse cells and THP-1 human cells were pretreated with **B8** for 2 h followed by LPS stimulation (0.5 μg/mL) for 6 h in triplicate experiments. Cells were then collected for total RNA extraction, followed by amplification for 40 cycles. As shown in Fig. 5, compound **B8** inhibited IL-6 mRNA transcription in mouse cells J774A.1 (A) and human cells THP-1 (B) in a dose-dependent manner. The

Table 1
Initial assessment of 4-HC and its derivatives (compounds **A1-A8**, **B1–B9**, and **C1–C8**) inhibiting the LPS-induced IL-6 release at a concentration of 10 μM.

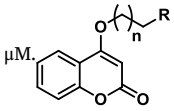

Compounds	n	R	Inhibition [a] (%, 10 μM)
A1	0		NA [b]
A2	0		4.36 ± 1.872
A3	0		50.35 ± 4.00
A4	0		17.46 ± 7.28
A5	1		17.53 ± 12.64
A6	2		NA
A7	2		39.02 ± 2.93
A8	2		NA
B1	1	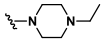	18.07 ± 9.79
B2	1	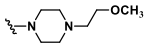	NA
B3	1	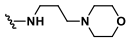	21.76 ± 6.77
B4	1	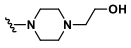	48.76 ± 4.58
B5	1	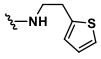	34.69 ± 4.27
B6	1		48.77 ± 2.38
B7	1	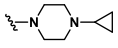	NA
B8	1	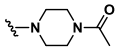	51.59 ± 2.43
B9	1	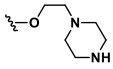	50.08 ± 8.12
C1	2	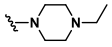	30.09 ± 5.82
C2	2	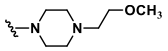	NA
C3	2	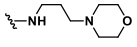	NA
C4	2	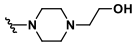	[a]1.26 [b] 4.82
C5	2	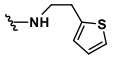	NA

Table 1 (*continued*)

Compounds	n	R	Inhibition [a] (%, 10 μM)
C6	2		NA
C7	2	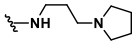	54.37 ± 5.34
C8	2	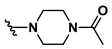	42.31 ± 3.16
4-HC			17.28 ± 12.31

[a] Data shown as mean ± SEM of three independent experiments.
[b] Exhibited no effect.

observed inhibition of IL-6 mRNA expression highlights a pivotal mechanism contributing to the anti-inflammatory properties of compound **B8**, suggesting its potential as a therapeutic agent for inflammatory conditions.

2.6. Effect of compound *B8* on the NF-κB pathway and MAPK signaling pathway

After observing the suppression of IL-6 release by compound **B8**, we proceeded to investigate its impact on the inflammation-associated TLR4-NF-κB/MAPK signaling pathway induced by LPS. Fig. 6A illustrates the basic mechanism through which LPS triggers the activation of the TLR4 pathway, which can be initiated by DAMPs (Damage-Associated Molecular Patterns) such as LPS and DSS. With the assistance of MD-2 protein, LPS binds to TLR4, activates TLR-4, transmits signals to cells, and activates intracellular transduction pathways, ultimately activating MyD88 [37,38]. The activated MyD88 along with MyD88 adapter protein analogues gathered in the receptor complex, leading to IRAK phosphorylation activation followed by signal transmission to TRAF6, which then activates IRAK1/4 [39,40]. Research indicates that TRAF6 stimulates IKKα, IKKβ and TAK1 to activate the corresponding NF-κB and MAPK pathways [41]. Through these pathways, inflammatory factors such as IL-6 are ultimately released, resulting in an inflammatory response [42]. Activation of the NF-κB pathway involves phosphorylation of P65 and degradation of IκB-α. Conversely, the phosphorylation of p38 and the phosphorylation of JNK are the key to the activation of MAPK signaling pathway. Therefore, we investigated the effects of compound **B8** on NF-κB pathway and MAPK pathway. In the NF-κB pathway, we tested the effect of **B8** on LPS-induced p-65 phosphorylation and IκBα degradation but observed no effect (Fig. S1). Subsequently, we assessed the inhibitory effect of compound **B8** on the LPS-induced JNK and p38 phosphorylation in the MAPK pathway. According to the results, compound **B8** did not inhibit JNK phosphorylation (Fig. S2). Interestingly, **B8** affected p38 phosphorylation (Fig. 6B). After stimulating mouse monocyte-macrophage-like cells with LPS, there was a significant increase in p38 phosphorylation levels, which were effectively attenuated by treatment with compound **B8**. These findings suggest that **B8** exerts a suppressive effect on the activation of the p38-MAPK signaling pathway.

2.7. Search for the target of compound *B8*

Currently, there is no established target for 4-HC, and no information is available regarding the targets of 4-HC derivatives in the context of LPS-induced inflammatory responses [43]. The search for targets of drugs or active compounds is necessary; and it is quite demanding. Many drugs and natural products have been confirmed to possess potent biological activity, yet their specific targets often remain unidentified. In this regard, identifying the targets for drugs or active compounds is a challenging and intricate task in the field of pharmacology and molecular biology. For example, metformin, a drug used for the treatment of

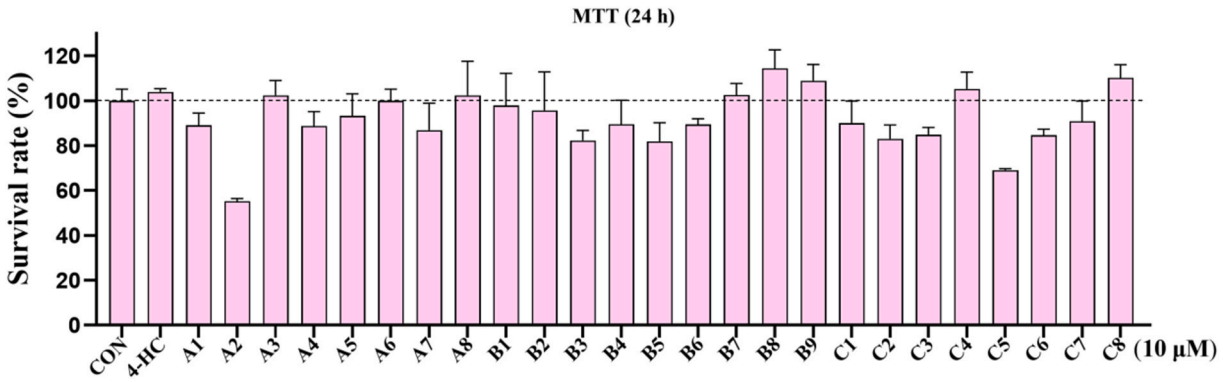

Fig. 3. Cell viability was determined using the MTT assay on J774A.1 cells, and results are presented as a percentage relative to the control group.

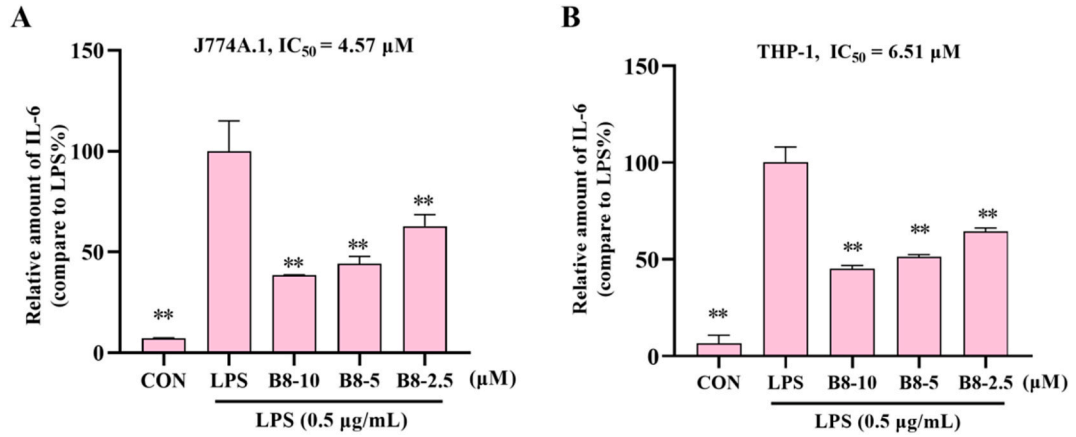

Fig. 4. The dose-dependent inhibitory effect of compound **B8** on the production of pro-inflammatory cytokine IL-6 on mouse cells J774A.1 (A) and human cells THP-1 (B) were pretreated with **B8** (10 μM), DMSO or gradient diluted **B8** for 30 min before LPS (0.5 μg/mL) treatment. After 24 h, 50 μL of medium was collected from each well of the cell culture plate and transferred to the 96-well plate. According to the instructions of the kit manufacturer, the absorbance (OD) value was measured with a microplate reader. The mean ± SEM value of the three copies was reported as a percentage of the LPS group value; compared with LPS group, $^{**}P < 0.01$.

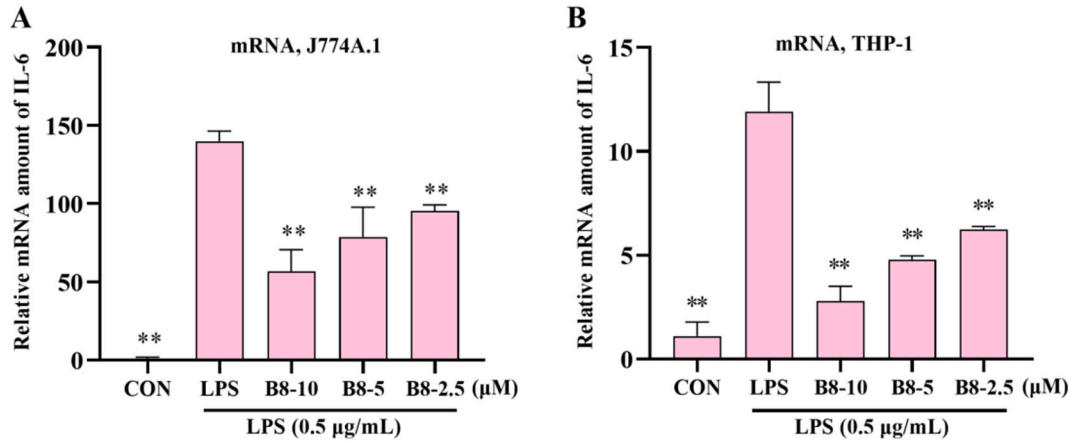

Fig. 5. Real-time qPCR analysis of compound **B8** on the inhibition of mRNA expression in a dose-dependent manner on IL-6 in mouse cells J774A.1 (A) and human cells THP-1 (B). Data are expressed as mean ± SEM, $^{**}p < 0.01$.

type 2 diabetes, had been available on the market for over 60 years without clear identification of its target. It wasn't until 2022 that a study published in *Nature* revealed that metformin exerts its effects on the lysosomal 5′-monophosphate (AMP)-activated protein kinase (AMPK) pathway through enhancer 2 (PEN2) at low doses [44].

Building upon prior experiments demonstrating **B8**'s modulation of the MAPK pathway, we initially chose over 30 proteins associated with this signaling cascade (such as TLR4, MD2, MyD88, IRAK1, IRAK4, JNK1, JNK2, JNK3, p38, TRAF6, TAK1, and TAB2, among others). We employed a procedure as our previous work in *J. Med. Chem* [45]. We listed the top 10 proteins based on the predicted docking scores, and Table 2 shows the scoring results.

Finally, we performed kinase inhibition experiments of **B8** on the top 5 kinases, including IRAK1, TAK1, JNK2, IKKβ, and p38 at 10 μM. The

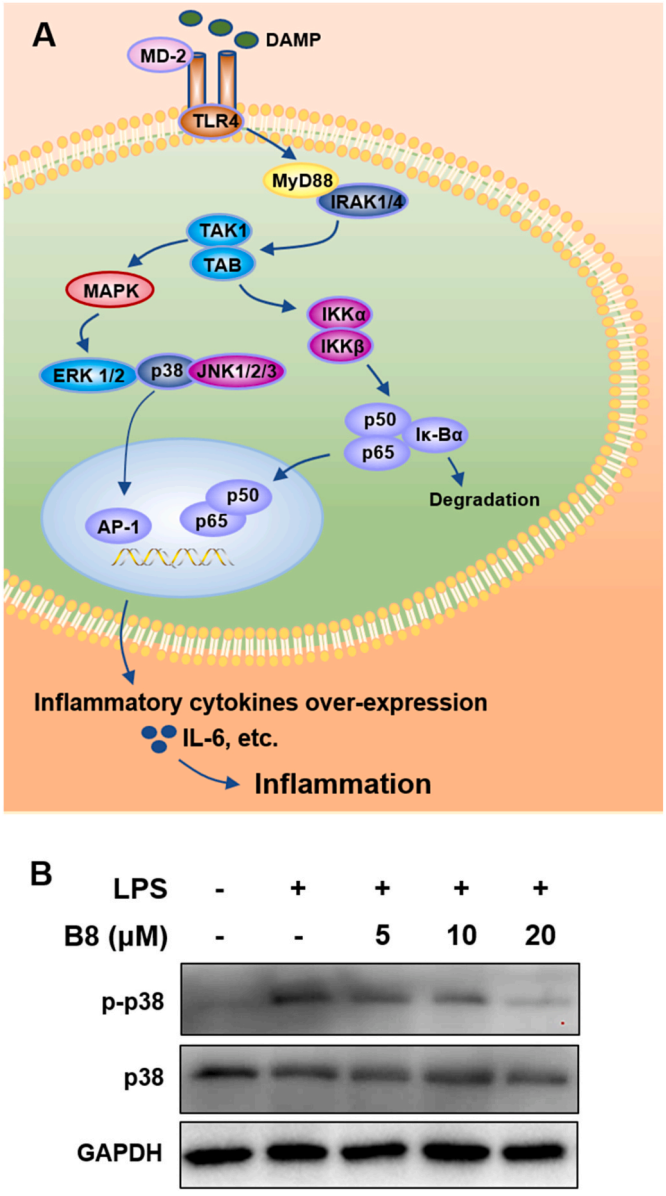

Fig. 6. The classic inflammatory pathway and the mechanism of action of **B8** were investigated. **(A)** Mechanism of the classical inflammatory pathway. **(B)** Compound **B8** can inhibit the activation of the MAPK pathway. J774A.1 cells were incubated with **B8** for 2 h and stimulated with LPS for 30 min. The protein levels of p-p38, p38, and GAPDH protein levels were detected by Western blot (WB).

Table 2
The top 10 proteins based on the predicted docking scores of **B8** and its inhibition rates on the top 5 kinases.

Protein	Docking Score	Inhibition rate (%)
IRAK1	−8.943	48.10
TAK1	−7.699	1.05
JNK2	−7.149	5.93
IKKβ	−6.213	−9.11
p38	−6.192	−12.74
IRAK4	−5.728	–
TAB2	−3.296	–
TRAF6	−2.989	–
p65	−2.692	–
Myd88	−1.464	–

results showed that **B8** inhibited IRAK1 by 48.10 %, and did not bind to TAK1, JNK2, IKKβ, and p38. Therefore, targeting on IRAK1 was identified as a key mechanism of **B8** for the anti-inflammatory activity. The inhibition rate is not very high, and so there may be other mechanism deserving to make further study in future. It is noteworthy that coumarin derivatives that bind to IRAK1 have not been reported previously, marking an important discovery for coumarin derivatives.

2.8. Molecular docking study of compound *B8*

To further study the mechanism of action of compound **B8**, we employed the IRAK1 protein (PDB: 6BFN) for docking research in Maestro. We optimized both protein and ligand, setting the docking frame around the original ligand of the protein. The docking results between compound **B8** and IRAK1 were then visualized using Pymol software (Fig. 7A). Fig. 7B shows the 2D docking results. We found that the coumarin group of **B8** acts as a hydrogen bond acceptor to form a hydrogen bond with the LEU291 residue. Furthermore, we also found that **B8** interacts with VAL226, ALA237 and LEU347 to produce Pi-Alkyl. In addition, the acetyl carbon atom of compound **B8** acts as a hydrogen bond acceptor to form a hydrogen bond with the GLU220 residue. These docking results offer insights into the three-dimensional binding mode of **B8** with the IRAK1 protein, emphasizing the specific interaction between **B8** and crucial amino acid residues. The presence of hydrogen bonds, Pi-Alkyl interactions, van der Waals forces, and carbon-hydrogen bonds underscores the potential significance of these interactions in modulating the anti-inflammatory properties of **B8**.

2.9. Compound *B8* alleviated LPS-induced ALI in mice

In an inflammatory ALI model, mice were orally administered a 20 mg/kg dose of compound **B8** three times at 12-h intervals to assess its effects. ALI was induced by intratracheal injection of 5 mg/kg LPS. The mice were euthanized after 6 h. Results demonstrated a substantial increase in protein content and neutrophil count in the Bronchoalveolar Lavage Fluid (BALF) following LPS administration (Fig. 8A and **D**). However, the protein levels and the number of neutrophils in BALF returned to normal levels after **B8** treatment. It has been established that LPS stimulates neutrophils, macrophages, and pulmonary vascular endothelial cells to release inflammatory factors, including IL-6, which can cause a localized inflammatory response in the lungs [48]. Therefore, this study was to detect the changes of IL-6 in BALF and IL-6 in serum of mice. Significant differences in IL-6 content were observed in both the BALF and serum of the **B8**-treated group compared to the LPS group, with serum IL-6 levels resembling those of the Dexamethasone (DXM) group (Fig. 8B and **C**).

We performed H&E staining and immunohistochemistry on lung sections (Fig. 9) to further validate the therapeutic effect on ALI. The LPS group showed classic pathological changes such as inflammatory infiltration, interstitial edema, thickening of the alveolar septum, elevated immune markers, and destruction of the alveolar cell structure. Compound **B8** significantly alleviated this impact, with a curative effect comparable to that of the DXM group. In conclusion, compound **B8** exerted a protective effect against the LPS-induced ALI.

2.10. Compound *B8* alleviated DSS-induced colitis in mice

We treated mice (C57BL/6) with **B8** (20 mg/kg), 4-HC (20 mg/kg), and 5-ASA (100 mg/kg) [46] for ten days to further verify the anti-inflammatory activity of **B8** *in vivo*. The mice were initially fed a liquid diet containing a 2.5 % DSS solution for the first seven days, followed by a switch to distilled water for the remaining three days. Throughout the ten-day period, observations were made regarding changes in body weight, fecal condition, and presence of hematochezia in the mice. After the ten-day period, the mice were euthanized. Colitis is a recognized inflammatory condition, with alterations in body weight,

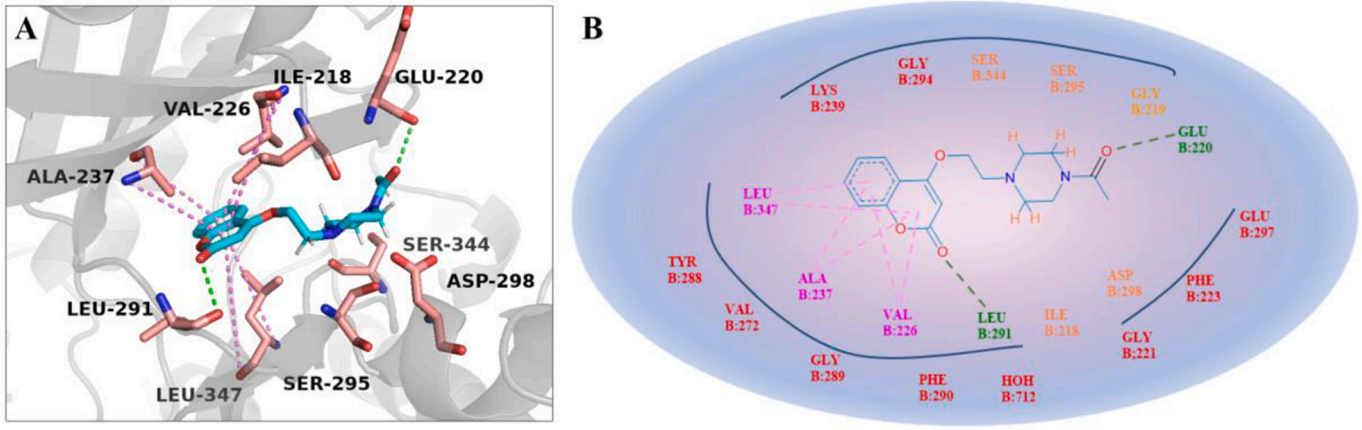

Fig. 7. (A) 3D docking view of **B8** with IRAK1 (PDB: 6BFN). **(B)** 2D docking view of **B8** with IRAK1 (PDB: 6BFN). Light-purple and green dotted lines represent the Pi-Alkyl and the hydrogen bond.

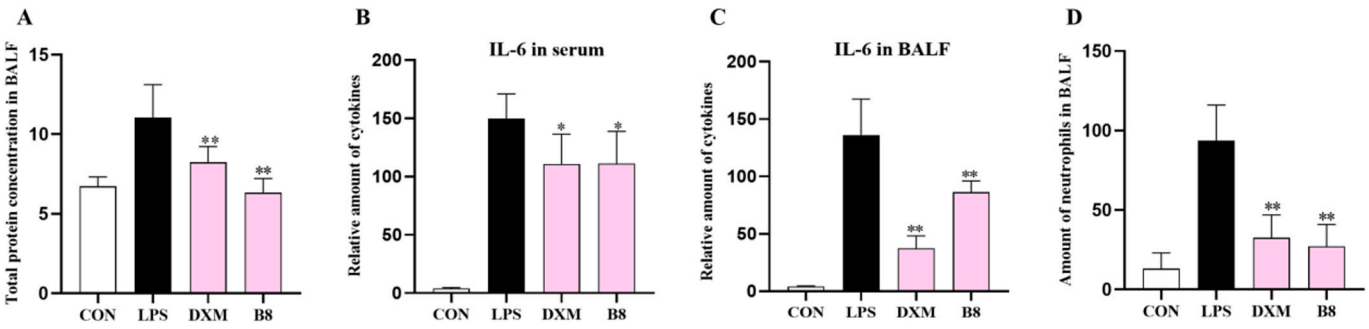

Fig. 8. The effect of compound **B8** on LPS-induced ALI in mice **B8** pretreatment inhibited LPS-induced ALI in mice. C57BL/6 mice were orally administered with **B8** (20 mg/kg) or DXM (20 mg/kg) three times at an interval of 12 h, followed by intratracheally injection of LPS (5 mg/kg). The mice were euthanized after 6 h, and lung specimens were collected. **(A)** Total protein concentration in BALF. **(B, C)** The IL-6 levels in serum and BALF were measured using the ELISA method. **(D)** Number of neutrophils in BALF. Data were shown as mean ± SEM, n = 6, *, $p < 0.05$; **, $p < 0.01$, compared with the LPS group.

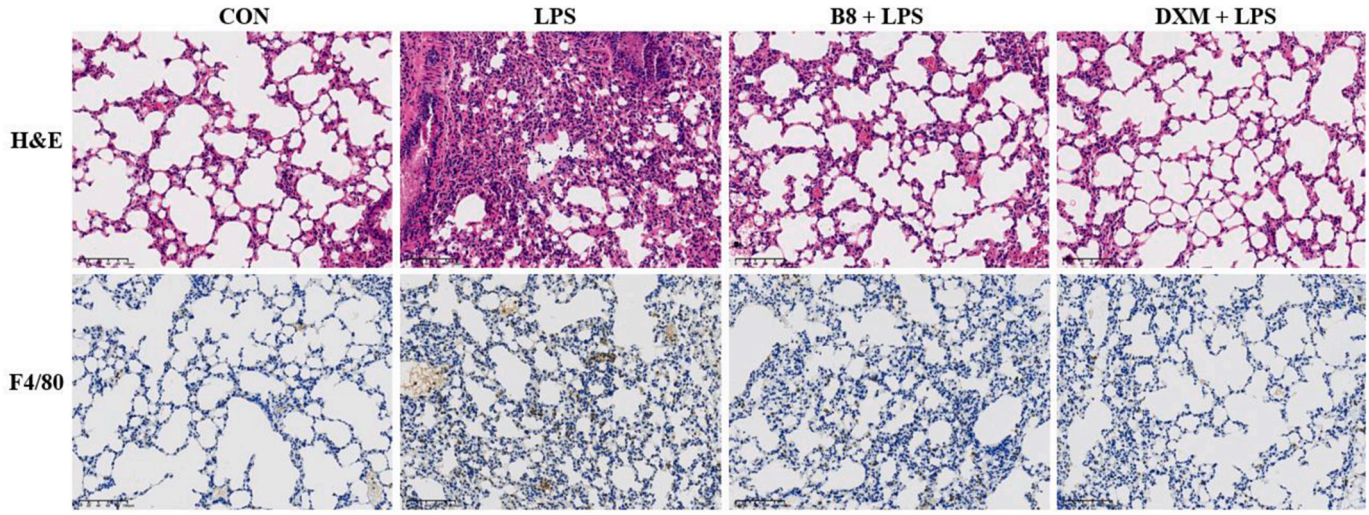

Fig. 9. Images of typical H&E staining and F4/80 immunohistochemical staining of the lung (original magnification × 20).

colon length, and disease index serving as pivotal indicators for assessing colitis progression. Our experimental results revealed that these three indicators were significantly better in **B8**-treated mice than in animals in the model and 4-HC groups (Fig. 10A, B, D, and **E**). Furthermore, the therapeutic effect was close to 5-ASA. Since IL-6 is also an important indicator of colitis [47], we assessed its levels in the serum of mice. Compared to the DSS group, the **B8**-treated mice could more significantly inhibit IL-6 release in plasma, implying that **B8** can alleviate colitis-related inflammation (Fig. 10C). The H&E staining of intestinal sections revealed that most of the crypts and goblet cells in the DSS group were destroyed (Fig. 11). Conversely, the **B8** group maintained the normal morphology of crypts and goblet cells, with **B8**

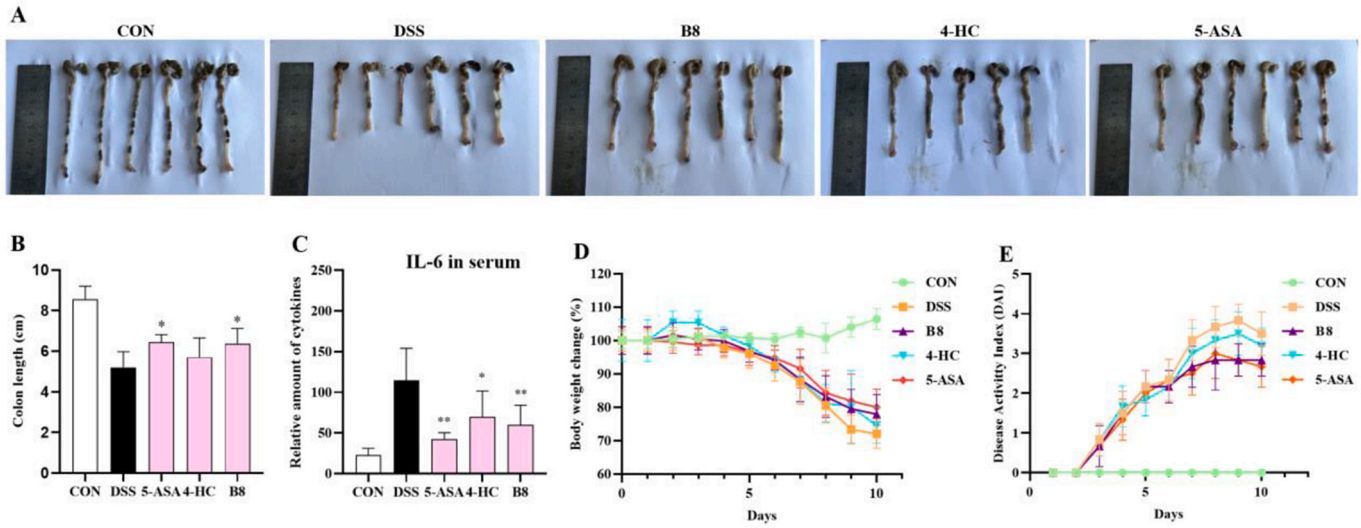

Fig. 10. Effect of compound **B8** on DSS-induced UC in mice. Mice (C57BL/6) were intragastrically treated with **B8** (20 mg/kg) for ten days. During this period, the mice received a liquid diet of 2.5 % DSS solution for the first seven days, which was later changed to distilled water in the last three days. The body weight, fecal status and hematochezia of the mice were recorded within ten days. The mice were euthanized ten days later, and the colons were removed. One mouse died in the 4-HC group on the ninth day. **(A)** Images of the colon length of mice in each group at the same scale. **(B)** Colon length of each group (n = 6/group). **(C)** IL-6 levels in the serum of each group of mice (n = 6/group). **(D)** The weight change rate of mice in each group over ten days (the ratio of the weight change of mice in each group to the weight of mice on the first day). **(E)** DAI scores of each group over ten days (n = 6/group). Data are expressed as mean ± SEM. Compared with the DSS group, *P < 0.05, **P < 0.001.

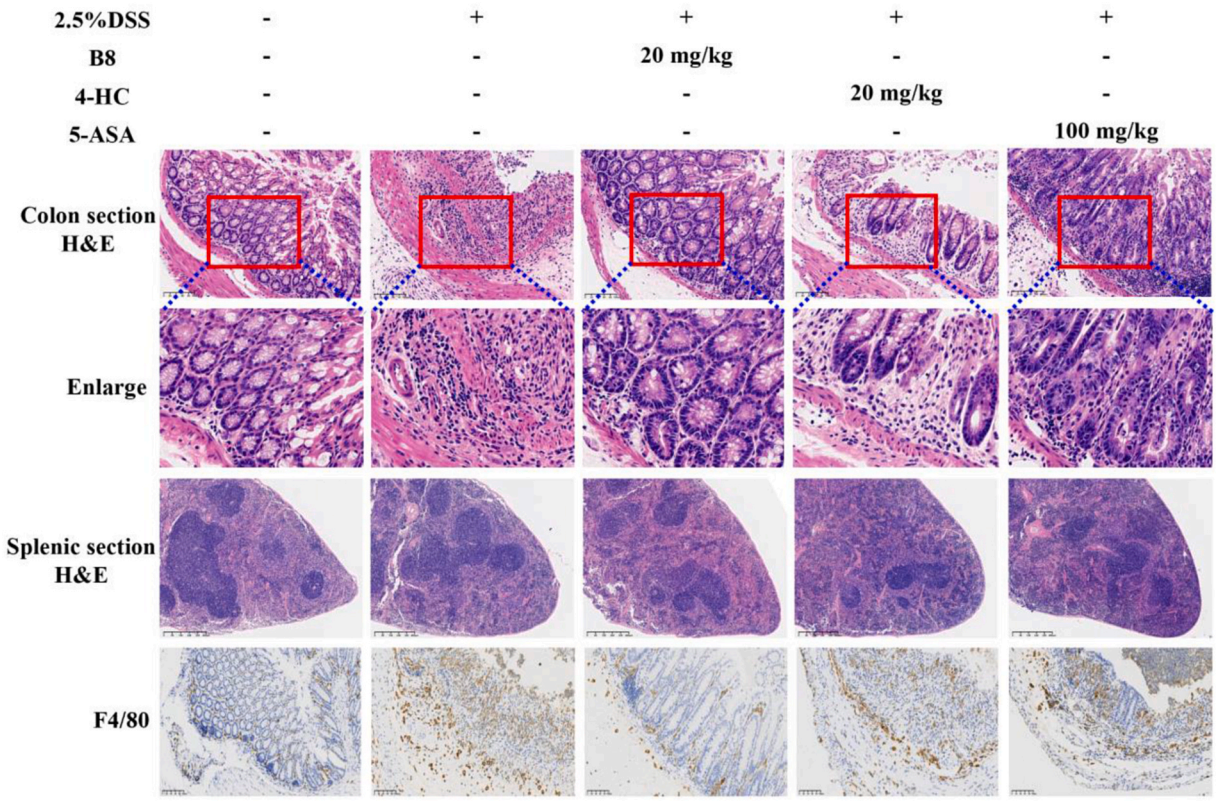

Fig. 11. Intestinal sections and spleens from each mouse group underwent H&E staining with meticulous attention to uniform positioning. Furthermore, intestinal sections were subjected to immunohistochemical staining for F4/80 at an original magnification of × 20 to enhance the analysis of the specimens.

demonstrating a superior effect compared to 4-HC and 5-ASA. Subsequently, the intestinal sections were immunohistochemically stained for F4/80, an inflammation-associated immune marker. According to the results, the population of F4/80 positive cells was significantly lower in the **B8** group than in the model, 4-HC, and 5-ASA groups (Fig. 11), confirming that **B8** could decelerate colitis-induced intestinal inflammation. The spleen, a crucial immune organ, typically exhibits a merging of the red and white pulp during colitis. Histological images from H&E staining of the spleen indicate that **B8** demonstrates potential in ameliorating this characteristic. Cumulatively, these observations

suggest that **B8** has a promising efficacy in alleviating DSS-induced colitis in mice.

2.11. Acute toxicity evaluation of compound *B8* on ICR mice

Subsequent acute toxicity assays were performed to further evaluate the *in vivo* safety profile of compound **B8**. On the initial day, mice were orally administered compound **B8** at doses of 1000 and 500 mg/kg. Subsequently, over a nine-day duration, the body weight of each mouse was diligently documented in the afternoons, with an untreated control group included for comparative analysis. No fatalities or severe adverse effects attributed to the drug were observed within any of the experimental cohorts during the study period. All groups displayed an initial decline in body weight on the first day, followed by a consistent upward trajectory thereafter (Fig. 12). Nonetheless, no statistically significant differences in body weight changes were found between the treated and control groups. The mice were humanely euthanized upon completion of the monitoring period, and their organs were harvested for histopathological examination via H&E staining. Fig. S3 (in supporting information) summarizes the findings, showing the absence of notable pathological alterations in mice organs obtained from both the high-dose and low-dose groups. These observations associate compound **B8** with low *in vivo* toxicity, highlighting its safety for administration.

2.12. Preliminary evaluation of the PK characteristics of compound *B8* in rats

Due to its promising anti-inflammatory activity of **B8** in both *in vivo* and *in vitro* studies, we conducted a preliminary pharmacokinetic study using **B8** on 16-week-old male SD rats. The plasma concentration-time profile of **B8** is depicted in Fig. 13. To calculate pharmacokinetic parameters for fitting, we employed Drug and Statistics (DAS) software 3.0 and non-compartmental models. Table 3 summarizes the results, indicating that the active compound **B8** achieved maximum plasma concentration within 0.67 h of oral administration, with a favorable $T_{1/2}$ value of 2.36 h and bioavailability (F) of 28.72 %.

3. Conclusions

Herein, 25 derivatives were designed and synthesized with 4-HC as the lead compound. The anti-inflammatory activity of this series of compounds was then evaluated, with 15 derivatives demonstrating superior anti-inflammatory activity compared to 4-HC. Among them, compound **B8** showed 3 time more active than 4-HC on IL-6 production, with IC_{50} values of 4.57 μM and 6.51 μM for IL-6 release from mouse cells J774A.1 and human cells THP-1, respectively. It was observed that

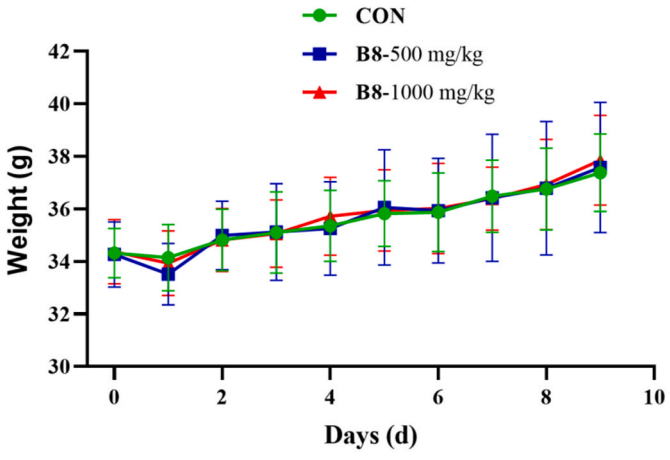

Fig. 12. Body weight of all mice (g) against time (day). Weight data were expressed as standard error of mean body weight (SEM).

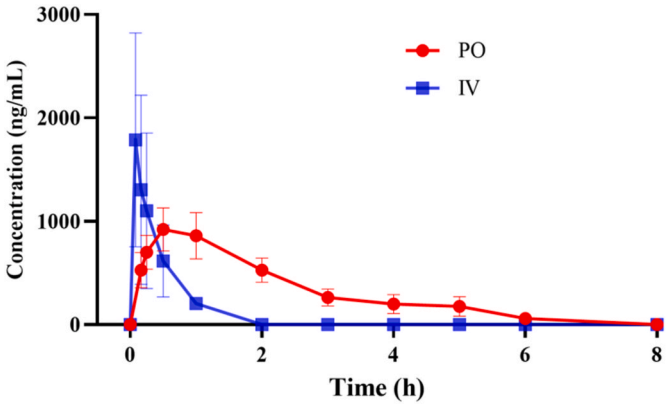

Fig. 13. Average blood concentration-time curve of **B8** in SD rats. For the oral administration, 13 time points (10 min, 15 min, 30 min, 1 h, 2 h, 3 h, 4 h, 5 h, 6 h, 8 h, 10 h, 12 h, and 24 h) were selected at which observations were recorded, and 14 time points (5 min, 10 min, 15 min, 30 min, 1 h, 2 h, 3 h, 4 h, 5 h, 6 h, 8 h, 10 h, 12 h, and 24 h) were selected for the intravenous administration.

Table 3
Pharmacokinetic parameters for compound **B8** in SD rats.

Parameters	iv (1 mg/kg)	po (10 mg/kg)
C_{max} (ng/mL)	2031.85	1014.61
$AUC_{(0-t)}$ (h*ng/mL)	929.43	2669.32
$AUC_{(0-\infty)}$ (h*ng/mL)	1019.26	3258.76
T_{max} (h)		0.67
$T_{1/2}$ (h)	0.31	2.36
F (%)		28.72

Data were expressed as mean concentrations in rat plasma (n = 3).

B8 could act on the MAPK pathway and targeting on IRAK1 was a key mechanism, which has not been previously reported and is an important finding for coumarin derivatives. In the ALI model, **B8** could reduce IL-6 release and inflammatory cell infiltration, thereby alleviating lung injury. In the DSS-induced mouse colitis model, we discovered that **B8** could significantly decelerate colon shortening and weight loss, significantly inhibit IL-6 production in the blood, and reduce intestinal damage. *In vivo* acute toxicity testing revealed that **B8** had no adverse effects on the body weight, behavior, or organ tissues of ICR mice at doses of 1000 mg/kg and 500 mg/kg. Moreover, **B8** exhibited favorable PK parameters in SD rats with a favorable $T_{1/2}$ value of 2.36 h and bioavailability (F) of 28.72 % for oral administration. Overall, **B8** is a potential candidate drug for treating ALI and colitis.

4. Experimental

4.1. Chemical synthesis

If not specified, all reagents and solvents utilized in the experiment were commercially acquired and used without any additional purification. The reaction was observed under ultraviolet light (254 nm) using a TLC analysis on a silica gel plate. For rapid column chromatography purification, Merck silica gel 60 (230–400 mesh ASTM) was employed. The melting points were determined using a Fisher Johns melting point meter without any adjustments. The ^{1}H and ^{13}C NMR spectra were recorded on a 400 MHz spectrometer bought from Bruker Corporation, Switzerland, with TMS serving as the internal reference. Mass spectrometry (MS) was conducted using an Agilent 1100 LC-MS system from Agilent, Palo Alto, CA, USA.

4.2. General procedure for the preparation of compounds *A1-A8*

4-HC (100 mg, 0.617 mmol), epoxybromopropane (101 μL,1.234

mmol), K_2CO_3 (256 mg, 1.855 mmol), and 2 mL of DMF were added to a 50 mL dry round-bottom flask. The mixture was reacted at 80 °C for 3 h, which was monitored by TLC. After the reaction, ethyl acetate was subjected to three extractions, followed by water wash (three times) and saturated salt water wash (one time). The organic layer was combined, dried with anhydrous $MgSO_4$. The $MgSO_4$ was filtered and the filtrate was concentrated under reduced pressure. The product **A1** was isolated and purified using a silica gel column with petroleum ether/ethyl acetate (10/1, v/v) in a yield of 48.3 %. The corresponding compounds **A1-A8** were obtained by the same method as **A1**.

4.2.1. 4-(Oxiran-2-ylmethoxy)-2H-1-benzopyran-2-one (A1)

White solid; yield: 48 %; purity, >95 %; m.p: 122–124 °C. ^{1}H NMR (400 MHz, $CDCl_3$) δ 7.83 (d, J = 7.1 Hz, 1H, H_6 coumarin ring), 7.72 (t, J = 7.8 Hz, 1H, H_8 coumarin ring), 7.35-7.25 (m, 2H, H_7, H_9 coumarin ring), 5.71 (s, 1H, H_3 coumarin ring), 4.32 (t, J = 7.6 Hz, 1H, -O-CH-), 4.23 (t, J = 7.3 Hz, 1H, -O-CH-), 2.76 (t, J = 5.2 Hz, 1H, -O-CH- ethylene oxide), 2.24-2.14 (m, 2H, -O-CH_2-ethylene oxide). ^{13}C NMR (100 MHz, $CDCl_3$) δ 165.3 (C_4 coumarin ring), 162.7 (C_2 coumarin ring), 153.3 (C_{10} coumarin ring), 133.1 (C_8 coumarin ring), 124.0 (C_7 coumarin ring), 123.1 (C_6 coumarin ring), 117.3 (C_9 coumarin ring), 115.4 (C_5 coumarin ring), 91.1 (C_3 coumarin ring), 70.0 (-O-C), 49.4 (-O-C ethylene oxide), 44.4 (-O-C ethylene oxide). LC-MS m/z: 219.06 [M + H] $^+$.

4.2.2. 4-(3-(2-(Piperazin-1-yl)ethoxy)propoxy)-2H-1-benzopyran-2-one (A2)

White solid; yield: 54 %; purity, >95 %; m.p: 178–180 °C. ^{1}H NMR (400 MHz, $CDCl_3$) δ 7.94 (d, J = 7.9 Hz, 1H, H_6 coumarin ring), 7.64 (t, J = 8.4 Hz, 1H, H_8 coumarin ring), 7.52-7.45 (m, 1H, Ar–H), 7.43-7.34 (m, 2H, H_7, H_9 coumarin ring), 7.30 (d, J = 7.7 Hz, 1H, Ar–H), 7.25 (d, J = 9.3 Hz, 1H, Ar–H), 7.21-7.13 (m, 1H, Ar–H), 5.83 (s, 1H, H_3 coumarin ring), 5.27 (s, 2H, -O-CH_2-). ^{13}C NMR (100 MHz, $CDCl_3$) δ 165.1 (C_4 coumarin ring), 164.3 (-C-F benzene ring), 162.7 (C_2 coumarin ring), 161.8 (-C-C- benzene ring), 153.3 (C_{10} coumarin ring), 132.7 (-C-C- benzene ring), 130.7 (C_8 coumarin ring), 130.6, (-C-C- benzene ring), 124.0 (C_7 coumarin ring), 123.1 (C_6 coumarin ring), 116.9 (C_9 coumarin ring), 116.0 (-C-C- benzene ring),115.9 (-C-C- benzene ring) 115.8 (C_5 coumarin ring), 91.0 (C_3 coumarin ring), 69.7 (-O-C-). LC-MS m/z: 293.0 [M + Na] $^+$.

4.2.3. 4-((3-Methoxybenzyl)oxy)-2H-chromen-2-one (A3)

White solid; yield: 59 %; purity, >95 %; m.p: 129–131 °C. ^{1}H NMR (400 MHz, $CDCl_3$) δ 7.91 (d, J = 7.9 Hz, 1H, H_6 coumarin ring), 7.59 (t, J = 7.8 Hz, 1H, H_8 coumarin ring), 7.42-7.34 (m, 2H, H_7, H_9 coumarin ring), 7.30 (t, J = 3.8 Hz, 1H, Ar–H), 7.06 (d, J = 7.6 Hz, 1H, Ar–H), 7.02 (s, 1H, Ar–H), 6.97 (d, J = 8.3 Hz, 1H, Ar–H), 5.81 (s, 1H, H_3 coumarin ring), 5.21 (s, 2H, -O-CH_2-), 3.88 (s, 3H, –OCH_3). ^{13}C NMR (100 MHz, $CDCl_3$) δ 165.3 (C_4 coumarin ring), 162.8 (C_2 coumarin ring), 160.0 (-C-O- benzene ring), 153.4 (C_{10} coumarin ring), 136.0 (-C-C- benzene ring), 132.5 (-C-C- benzene ring), 130.0 (C_8 coumarin ring), 124.0 (C_7 coumarin ring), 123.2 (C_6 coumarin ring), 120.0 (-C-C- benzene ring), 116.8 (C_9 coumarin ring), 115.7 (C_5 coumarin ring), 114.0 (-C-C- benzene ring), 113.4 (-C-C- benzene ring), 91.3 (C_3 coumarin ring), 71.0 (-O-C-), 55.4 (-O-CH_3). LC-MS m/z: 305.1 [M + Na] $^+$.

4.2.4. 4-((3,5-Dimethylbenzyl)oxy)-2H-chromen-2-one (A4)

White solid; yield: 58 %; purity, >95 %; m.p: 110–114 °C. ^{1}H NMR (400 MHz, CDCl3) δ 7.91 (d, J = 7.9 Hz, 1H, H_6 coumarin ring), 7.59 (t, J = 7.8 Hz, 1H, H_8 coumarin ring), 7.38-7.28 (m, 3H, H_7, H_9 coumarin ring, Ar–H), 7.10-7.05 (m, 3H, Ar–H × 3), 5.81 (s, 1H, H_3 coumarin ring), 5.17 (s, 2H, -O-CH_2-), 2.39 (s, 6H, –CH_3 × 2). ^{13}C NMR (100 MHz, $CDCl_3$) δ 165.3 (C_4 coumarin ring), 162.8 (C_2 coumarin ring), 160.0 (-C-C- benzene ring), 153.4 (C_{10} coumarin ring), 135.9 (-C-C- benzene ring), 132.5 (-C-C- benzene ring), 130.0 (C_8 coumarin ring), 124.0 (C_7 coumarin ring), 123.2 (C_6 coumarin ring), 120.0 (-C-C- benzene ring), 116.8 (C_9 coumarin ring), 115.7 (C_5 coumarin ring), 114.0 (-C-C- benzene ring), 113.4 (-C-C- benzene ring), 91.3 (C_3 coumarin ring), 71.0 (-O-C-), 55.4 × 2 (-C-CH_3 × 2). LC-MS m/z: 303.0 [M + Na] $^+$.

4.2.5. 4-(2-Morpholinoethoxy)-2H-1-benzo-pyran-2-one (A5)

Yellow solid; yield: 50 %; purity, >95 %; m.p: 118–120 °C. ^{1}H NMR (400 MHz, $CDCl_3$) δ 7.69 (d, J = 7.7 Hz, 1H, H_6 coumarin ring), 7.45 (t, J = 7.7 Hz, 1H, H_8 coumarin ring), 7.22-7.14 (m, 2H, H_7, H_9 coumarin ring), 5.61 (s, 1H, H_3 coumarin ring), 4.19 (t, J = 5.0 Hz, 2H, –OCH_2-), 3.70-3.60 (m, 4H, -O-CH_2 × 2, morpholine ring), 2.85 (t, J = 5.0 Hz, 2H, –CH_2-), 2.59-2.49 (m, 4H, -N-CH_2 × 2, morpholine ring). ^{13}C NMR (100 MHz, $CDCl_3$) δ 165.4 (C_4 coumarin ring), 162.6 (C_2 coumarin ring), 153.2 (C_{10} coumarin ring), 132.4 (C_8 coumarin ring), 123.9(C_7 coumarin ring), 123.0 (C_6 coumarin ring), 116.6 (C_9 coumarin ring), 115.5 (C_5 coumarin ring), 90.6 (C_3 coumarin ring), 67.4 (-O-C-), 66.8 × 2 (-O-C × 2 morpholine ring), 56.7 (-C-N-), 53.9 × 2 (-N-C × 2 morpholine ring). LC-MS m/z: 298.1 [M + Na] $^+$.

4.2.6. 4-(3-(Dimethylamino)propoxy)-2H-1-benzopyran-2-one (A6)

Yellow oily; yield: 48 % purity, >95 %. ^{1}H NMR (400 MHz, $CDCl_3$) δ 7.81 (d, J = 7.9 Hz, 1H, H_6 coumarin ring), 7.54 (t, J = 7.8 Hz 1H, H_8 coumarin ring), 7.35-7.21 (m, 2H, H_7, H_9 coumarin ring), 5.69 (s, 1H, H_3 coumarin ring), 4.19 (t, J = 5.9 Hz, 2H, –OCH_2-), 2.59-2.43 (m, 2H, -N-CH_2-), 2.28 (s, 6H, -N-CH_3 × 2), 2.12-2.02 (m, 2H, –CH_2-). ^{13}C NMR (100 MHz, $CDCl_3$) δ 165.7 (C_4 coumarin ring), 163.0 (C_2 coumarin ring), 153.3 (C_{10} coumarin ring), 132.5 (C_8 coumarin ring), 123.9 (C_7 coumarin ring), 123.0 (C_6 coumarin ring), 116.7 (C_9 coumarin ring), 115.8 (C_5 coumarin ring), 90.5 (C_3 coumarin ring), 67.6 (-O-C-), 55.9 (-C-N-), 45.4 × 2 (-N-CH_3 × 2), 26.8 (-C-C-). LC-MS m/z: 270.1 [M + Na] $^+$.

4.2.7. 4-(3-(Pyrrolidin-1-yl)propoxy)-2H-1-benzopyran-2-one (A7)

Yellow solid; yield: 53 %; purity, >95 %; m.p: 59–61 °C. ^{1}H NMR (400 MHz, $CDCl_3$) δ 7.83 (d, J = 8.5 Hz, 1H, H_6 coumarin ring), 7.73 (d, J = 5.6 Hz, 1H, H_8 coumarin ring), 7.62-7.50 (m, 2H, H_7, H_9 coumarin ring), 5.71 (s, 1H, H_3 coumarin ring), 4.32 (t, J = 6.7 Hz, 2H, –OCH_2-), 2.76 (t, J = 7.4 Hz, 2H, -N-CH_2), 2.66 (t, J = 5.5 Hz 2H, -N-CH_2), 2.25-2.13 (m, 2H, -N-CH_2), 1.88-1.85 (m, 2H, –CH_2- tetrahydropyrrole ring), 1.79-1.66 (m, 2H, –CH_2- tetrahydropyrrole ring), 1.48-1.43 (m, 2H, –CH_2-).

4.2.8. 4-(2-Morpholinoethoxy)-2H-1-benzo-pyran-2-one (A8)

White solid; yield: 48 %; purity, >95 %; m.p: 113–114 °C. ^{1}H NMR (400 MHz, $CDCl_3$) δ 7.83 (d, J = 9.4 Hz, 1H, H_6 coumarin ring), 7.57 (t, J = 8.6 Hz, 1H, H_8 coumarin ring), 7.36-7.27 (m, 2H H_7, H_9 coumarin ring), 5.73 (s, 1H, H_3 coumarin ring), 4.24 (t, J = 6.3 Hz, 2H, –OCH_2-), 3.81-3.69 (m, 4H, –OCH_2 × 2 morpholine ring), 2.59 (t, J = 7.1 Hz, 2H, –CH_2-), 2.55-2.48 (m, 4H, -N-CH_2 × 2 morpholine ring), 2.17-2.08 (m, 2H, –CH_2-). ^{13}C NMR (100 MHz, $CDCl_3$) δ 165.6 (C_4 coumarin ring), 163.0 (C_2 coumarin ring), 153.4 (C_{10} coumarin ring), 132.4 (C_8 coumarin ring), 123.9 (C_7 coumarin ring), 122.9 (C_6 coumarin ring), 116.9 (C_9 coumarin ring), 115.8 (C_5 coumarin ring), 90.6 (C_3 coumarin ring), 67.5 (-O-C-), 66.9 × 2 (-O-C × 2 morpholine ring), 55.1 (-C-N-), 53.8 × 2 (-N-C × 2 morpholine ring), 25.7 (-C-C-). LC-MS m/z: 312.1 [M + Na] $^+$.

4.3. General procedure for the preparation of intermediates a1, b1

In a 50 mL dry round-bottom flask, 4-HC (100 mg, 0.617 mmol) was combined with either 1,2-dibromoethane (160 μL, 1.851 mmol) or 1,3-dibromopropane (187 μL, 1.851 mmol), along with K_2CO_3 (256 mg, 1.855 mmol). 2 mL of DMF was slowly added, the mixture was reacted at 80 °C for 3.5 h. After the reaction, ethyl acetate was used to extract for three times, followed by washing with distilled water (three times) and saturated salt water (one time). The organic layer was combined and dried with anhydrous $MgSO_4$. The $MgSO_4$ was filtered and the filtrate was concentrated under reduced pressure. The intermediates **a1** (yield:

58 %) and **b1** (yield: 59 %) were separated by silica gel column chromatography using petroleum ether/ethyl acetate (10/1, v/v).

4.3.1. 4-(2-Bromoethoxy)-2H-1-benzopyran-2-one (a1)

White solid; yield: 58 %; m.p: 160–162 °C. ^{1}H NMR (400 MHz, $CDCl_3$) δ 7.89 (d, J = 7.9 Hz, 1H, H_6 coumarin ring), 7.59 (t, J = 8.0 Hz, 1H, H_8 coumarin ring), 7.39-7.26 (m, 2H, H_7, H_9 coumarin ring), 5.70 (s, 1H, H_3 coumarin ring), 4.48 (t, J = 5.8 Hz, 2H, –OCH_2-), 3.79 (t, J = 5.8 Hz, 2H, –CH_2Br). ^{13}C NMR (100 MHz, $CDCl_3$) δ 164.9 (C_4 coumarin ring), 162.6 (C_2 coumarin ring), 153.4 (C_{10} coumarin ring), 132.7 (C_8 coumarin ring), 124.1 (C_7 coumarin ring), 123.1 (C_6 coumarin ring), 116.8 (C_9 coumarin ring), 115.3 (C_5 coumarin ring), 90.9 (C_3 coumarin ring), 68.5 (-O-C-), 27.7 (-C-Br).

4.3.2. 4-(3-Bromopropoxy)-2H-1-benzopyran-2-one (b1)

White solid; yield: 59 %; m.p: 112–113 °C. ^{1}H NMR (400 MHz, $CDCl_3$) δ 7.82 (d, J = 7.9 Hz, 1H, H_6 coumarin ring), 7.58 (t, J = 8.6 Hz, 1H, H_8 coumarin ring), 7.36-7.28 (m, 2H H_7, H_9 coumarin ring), 5.75 (s, 1H, H_3 coumarin ring), 4.33 (t, J = 5.8 Hz, 2H, –OCH_2-), 3.66 (t, J = 6.3 Hz, 2H, –CH_2Br), 2.52-2.45 (m, 2H, –CH_2-). ^{13}C NMR (100 MHz, $CDCl_3$) δ 165.3 (C_4 coumarin ring), 162.7 (C_2 coumarin ring), 153.4 (C_{10} coumarin ring), 132.5 (C_8 coumarin ring), 124.0 (C_7 coumarin ring), 122.9 (C_6 coumarin ring), 116.9 (C_9 coumarin ring), 115.6 (C_5 coumarin ring), 90.9 (C_3 coumarin ring), 66.8 (-O-C-), 31.5 (-C-Br), 28.9 (-C-C-).

4.4. General procedure for the preparation of compounds B1–B9, C1–C8

1-Ethylpiperazine (50 μL,0.39 mmol) was dissolved in 2 mL DMF in a 50 mL dry round-bottom flask. Next, K_2CO_3 (161.46 mg, 1.17 mmol) was added followed by addition of the intermediate **a1** (104.91 mg, 0.39 mmol) or **b1** (110.37 mg, 0.39 mmol). The flask was placed in a magnetically heated stirrer at 80 °C for 4 h. Subsequently, ethyl acetate was used to extract three times, followed by three times wash with distilled water and one time wash with saturated salt water. The organic layer was combined, and dried using anhydrous $MgSO_4$. After filtration to remove $MgSO_4$, the filtrate was concentrated under reduced pressure. Subsequently, separation was achieved using DCM/MeOH (100/1, v/v) and purification was performed through a silica gel column, leading to the preparation of the final products **B1** (yield: 58 %) and **C1** (yield: 50 %). Products **B1–B9** and **C1–C9** were prepared following the same procedure.

4.4.1. 4-(2-(4-Ethylpiperazin-1-yl)ethoxy)-2H-1-benzopyran-2-one (B1)

Yellow oily; yield: 58 %. purity, >95 %. ^{1}H NMR (400 MHz, $CDCl_3$) δ 7.78 (d, J = 7.9 Hz, 1H, H_6 coumarin ring), 7.53 (t, J = 7.8 Hz, 1H, H_8 coumarin ring), 7.31-7.23 (m, 2H, H_7, H_9 coumarin ring), 5.67 (s, 1H, H_3 coumarin ring), 4.25 (t, J = 5.5 Hz, 2H, –OCH_2-), 2.93 (t, J = 5.5 Hz, 2H, C–CH_2–N), 2.79-2.46 (m, 8H, piperazine ring), 2.43-2.37 (m, 2H, -N-CH_2-), 1.07 (t, J = 7.2 Hz, 3H, –CH_3). ^{13}C NMR (100 MHz, $CDCl_3$) δ 165.5 (C_4 coumarin ring), 162.9 (C_2 coumarin ring), 153.3 (C_{10} coumarin ring), 132.4 (C_8 coumarin ring), 123.9 (C_7 coumarin ring), 123.0 (C_6 coumarin ring), 116.7 (C_9 coumarin ring), 115.6 (C_5 coumarin ring), 90.6 (C_3 coumarin ring), 67.6 (-O-C-), 56.3 (-C-N-), 53.5 × 2 (-N-C × 2 piperazine ring), 52.7 × 2 (-C-N × 2 piperazine ring), 52.2 (-N-C), 11.9 (C–C). LC-MS *m/z*: 325.1 [M + Na] $^+$.

4.4.2. 4-(2-(4-(2-Methoxyethyl)piperazin-1-yl)ethoxy)-2H-1-benzopyran-2-one (B2)

White solid; yield: 51 %; purity, >95 %; m.p: 96–97 °C. ^{1}H NMR (400 MHz, $CDCl_3$) δ 7.80 (d, J = 7.9 Hz, 1H, H_6 coumarin ring), 7.55 (t, J = 8.1 Hz, 1H, H_8 coumarin ring), 7.34-7.24 (m, 2H, H_7, H_9 coumarin ring), 5.68 (s, 1H, H_3 coumarin ring), 4.27 (t, J = 5.6 Hz, 2H, –OCH_2-), 3.52 (t, J = 5.6 Hz, 2H, –OCH_2-), 3.35 (s, 3H, –OCH_3), 2.95 (t, J = 5.6 Hz, 2H, –CH_2-N-), 2.74-2.66 (m, 4H, –CH_2 × 2 piperazine ring), 2.62-2.54 (m, 6H, –CH_2 × 2 piperazine ring, -N-CH_2-). ^{13}C NMR (100 MHz, $CDCl_3$) δ 165.5 (C_4 coumarin ring), 162.9 (C_2 coumarin ring), 153.3 (C_{10} coumarin ring), 132.4 (C_8 coumarin ring), 123.9 (C_7 coumarin ring), 123.1 (C_6 coumarin ring), 116.8 (C_9 coumarin ring), 115.7 (C_5 coumarin ring), 90.6 (C_3 coumarin ring), 70.0 (-C-O-), 67.6 (-O-C-), 58.9 (-O-CH_3), 57.8 (-C-N-), 56.3 (-N-C-), 53.5 × 2 (-N-C × 2 piperazine ring), 53.4 × 2 (-N-C × 2 piperazine ring). LC-MS *m/z*: 355.1 [M + Na] $^+$.

4.4.3. 4-(2-((3-Morpho-linopropyl)amino)ethoxy)-2H-1-benzopyran-2-one (B3)

Yellow oily; yield: 46 %; purity, >95 %. ^{1}H NMR (400 MHz, $CDCl_3$) δ 8.20 (d, J = 7.9 Hz, 1H, H_6 coumarin ring), 7.52 (t, J = 8.1 Hz, 1H, H_8 coumarin ring), 7.36-7.27 (m, 2H, H_7, H_9 coumarin ring), 5.77 (s, 1H, H_3 coumarin ring), 4.02 (t, J = 4.9 Hz, 2H, –OCH_2-), 3.77-3.72 (m, 4H, –OCH_2 × 2 morpholine ring), 3.52-3.44 (m, 2H, –CH_2-N-), 2.53-2.41 (m, 8H, -N-CH_2 × 2 coumarin ring, -N-CH_2 × 2), 1.96-1.82 (m, 2H, –CH_2-). ^{13}C NMR (100 MHz, $CDCl_3$) δ 162.5 (C_4 coumarin ring), 159.4 (C_2 coumarin ring), 154.4 (C_{10} coumarin ring), 131.5 (C_8 coumarin ring), 125.6 (C_7 coumarin ring), 123.5 (C_6 coumarin ring), 117.9 (C_9 coumarin ring), 116.9 (C_5 coumarin ring), 97.7 (C_3 coumarin ring), 66.7 (-O-C-), 66.0 × 2 (-C-O × 2 morpholine ring), 56.4 × 2 (-N-C × 2 morpholine ring), 45.6 (-C-N-), 44.7 (-C-N-), 42.5 (-N-C), 21.0 (C–C). LC-MS *m/z*: 355.1 [M + Na] $^+$.

4.4.4. 4-(2-(4-(2-Hydroxyethyl)piperazin-1-yl)ethoxy)-2H-1-benzopyran-2-one (B4)

White solid; yield: 60.1 %; purity, >95 %; m.p: 80–82 °C. ^{1}H NMR (400 MHz, $CDCl_3$) δ 7.83 (d, J = 7.9 Hz, 1H, H_6 coumarin ring), 7.59 (t, J = 7.8 Hz, 1H, H_8 coumarin ring), 7.38-7.30 (m, 2H, H_7, H_9 coumarin ring), 5.72 (s, 1H, H_3 coumarin ring), 4.30 (t, J = 5.4 Hz, 2H, –OCH_2-), 3.69 (t, J = 5.2 Hz, 2H, –CH_2-O-), 2.99 (t, J = 5.4 Hz, 2H, -N-CH_2-), 2.82-2.60 (m, 10H, -N-CH_2 × 4 piperazine ring, -N-CH_2). ^{13}C NMR (100 MHz, $CDCl_3$) δ 167.7 (C_4 coumarin ring), 162.9 (C_2 coumarin ring), 153.3 (C_{10} coumarin ring), 128.8 (C_8 coumarin ring), 124.0 (C_7 coumarin ring), 123.0 (C_6 coumarin ring), 116.8 (C_9 coumarin ring), 115.7 (C_5 coumarin ring), 90.7 (C_3 coumarin ring), 65.6 (-O-C-), 59.3 (-C-OH), 57.8 (-N-C-), 56.3 (-C-N-), 53.6 × 2 (-N-C × 2 piperazine ring), 52.8 × 2 (-N-C × 2 piperazine ring). LC-MS *m/z*: 355.1 [M + Na] $^+$.

4.4.5. 4-(2-((2-(Thiophen-2-yl)ethyl)amino)ethoxy)-2H-1-benzopyran-2-one (B5)

Yellow oily; yield: 41 %; purity, >95 %. ^{1}H NMR (400 MHz, $CDCl_3$) δ 7.92-7.76 (m, 1H, H_6 coumarin ring), 7.55 (d, J = 7.7 Hz, 1H, H_8 coumarin ring), 7.38-7.32 (m, 1H, -S-CH- thiophene ring), 7.29-7.17 (m, 2H, H_7, H_9 coumarin ring), 7.10-6.96 (m, 1H, -CH- thiophene ring), 6.89 (d, J = 3.1 Hz, 1H, -CH- thiophene ring), 5.74 (s, 1H, H_3 coumarin ring), 4.45-4.27 (m, 2H, –OCH_2-), 3.42-2.97 (m, 6H, -N-CH_2 × 2, –CH_2-). ^{13}C NMR (100 MHz, $CDCl_3$) δ 165.3 (C_4 coumarin ring), 162.7 (C_2 coumarin ring), 153.3 (C_{10} coumarin ring), 140.8 (-S-C- thiophene ring), 132.6 (C_8 coumarin ring), 127.18 (-C-C- thiophene ring), 125.68 (-C-C- thiophene ring), 124.18 (-S-C- thiophene ring), 124.0 (C_7 coumarin ring), 123.2 (C_6 coumarin ring), 116.8 (C_9 coumarin ring), 115.4 (C_5 coumarin ring), 90.9 (C_3 coumarin ring), 67.6 (-O-C-), 50.5 (-C-N-), 47.2 (-N-C-), 29.7 (C–C). LC-MS *m/z*: 338.1 [M + Na] $^+$.

4.4.6. 4-(2-(3-Methylpiperidin-1-yl)ethoxy)-2H-1-benzopyran-2-one (B6)

Yellow oily; yield: 58 %; purity, >95 %. ^{1}H NMR (400 MHz, $CDCl_3$) δ 7.81 (d, J = 7.8 Hz, 1H, H_6 coumarin ring), 7.55 (t, J = 8.0 Hz, 1H, H_8 coumarin ring), 7.33-7.25 (m, 2H, H_7, H_9 coumarin ring), 5.70 (s, 1H, H_3 coumarin ring), 4.28 (t, J = 5.8 Hz, 2H, –OCH_2-), 2.99-2.89 (m, 4H, -N-CH_2 × 2), 2.13-2.06 (m, 2H, -N-CH_2-), 1.84-1.61 (m, 5H, –CH_2 × 2 piperidine ring, -CH- piperidine ring), 0.88 (d, J = 6.3 Hz, 3H, –CH_3). ^{13}C NMR (100 MHz, $CDCl_3$) δ 165.5 (C_4 coumarin ring), 162.9 (C_2 coumarin ring), 153.3 (C_{10} coumarin ring), 132.4 (C_8 coumarin ring), 123.9 (C_7 coumarin ring), 123.1 (C_6 coumarin ring), 116.8 (C_9 coumarin ring), 115.7 (C_5 coumarin ring), 90.6 (C_3 coumarin ring), 67.5 (-O-C-), 62.4 (-N-C- piperidine ring), 56.7 (-N-C- piperidine ring), 54.4 (-C-N- piperidine ring), 32.6 (-C-C- piperidine ring), 31.0 (-C-C- piperidine ring),

25.4 (-C-C- piperidine ring), 19.7 (-CH_3). LC-MS *m/z*: 310.1 [M + Na] $^+$.

4.4.7. 4-((3-Fluorobenzyl)oxy)-2H-chromen-2-one (B7)

White solid; yield: 43 %; purity, >95 %; m.p: 127–130 °C. ^{1}H NMR (400 MHz, $CDCl_3$) δ 7.83 (d, *J* = 7.8 Hz, 1H, H_6 coumarin ring), 7.58 (t, *J* = 7.9 Hz, 1H, H_8 coumarin ring), 7.40-7.30 (m, 2H, H_7, H_9 coumarin ring), 5.71 (s, 1H, H_3 coumarin ring), 4.30 (t, *J* = 5.6 Hz, 2H, –OCH_2-), 2.97 (t, *J* = 5.6 Hz, 2H, –CH_2-N-), 2.80-2.58 (m, 8H, -N-CH_2 × 4 piperazine ring), 1.72-1.60 (m, 1H, -N-CH- cyclopropane), 0.53-0.41 (m, 4H, –CH_2 × 2 cyclopropane). ^{13}C NMR (100 MHz, $CDCl_3$) δ 165.6 (C_4 coumarin ring), 162.9 (C_2 coumarin ring), 153.3 (C_{10} coumarin ring), 132.4 (C_8 coumarin ring), 123.9 (C_7 coumarin ring), 123.1 (C_6 coumarin ring), 116.8 (C_9 coumarin ring), 90.7 (C_3 coumarin ring), 67.6 (-O-C-), 56.3 (-C-N-), 53.5 × 2 (-N-C × 2 piperazine ring), 53.2 × 2 (-C-N × 2 piperazine ring), 38.43 (-N-C- cyclopropane), 5.73 × 2 (-C-C- cyclopropane). LC-MS *m/z*: 315.1 [M + H] $^+$.

4.4.8. 4-(2-(4-Acetylpiperazin-1-yl)ethoxy)-2H-chromen-2-onee (B8)

Yellowish solid; yield: 41 %; purity, >95 %; m.p: 133–134 °C. ^{1}H NMR (400 MHz, $CDCl_3$) δ 7.81 (d, *J* = 7.9 Hz, 1H, H_6 coumarin ring), 7.59 (t, *J* = 7.8 Hz, 1H, H_8 coumarin ring), 7.38-7.30 (m, 2H, H_7, H_9 coumarin ring), 5.72 (s, 1H, H_3 coumarin ring), 4.30 (t, *J* = 5.4 Hz, 2H, –OCH_2-), 3.72-3.64 (m, 2H, –CH_2-N- hydrogen on piperazine near carbonyl group), 3.56-3.50 (m, 2H, –CH_2-N- hydrogen on piperazine near carbonyl group), 2.99 (t, *J* = 5.4 Hz, 2H, –CH_2-N-), 2.68-2.58 (m, 4H, –CH_2-N × 2 hydrogen on the piperidine away from the carbonyl group), 2.13 (s, 3H, –CH_3). ^{13}C NMR (100 MHz, $CDCl_3$) δ 168.9 (-C=O), 165.4 (C_4 coumarin ring), 162.8 (C_2 coumarin ring), 153.4 (C_{10} coumarin ring), 132.6 (C_8 coumarin ring), 124.0 (C_7 coumarin ring), 122.9 (C_6 coumarin ring), 116.9 (C_9 coumarin ring), 115.6 (C_5 coumarin ring), 90.8 (C_3 coumarin ring), 67.5 (-O-C-), 56.2 (-C-N-), 53.6 (-C-N- carbon on piperazine near carbonyl group), 53.3 (-C-N- carbon on piperazine near carbonyl group), 46.2 (-C-N- carbon on the piperidine away from the carbonyl group), 41.4 (-C-N- carbon on the piperidine away from the carbonyl group), 21.3 (-CH_3). LC-MS *m/z*: 339.2 [M + H] $^+$.

4.4.9. 4-(3-((3-Morpho-linopropyl)amino)propoxy)-2H-1-benzopyran-2-one (B9)

White solid; yield: 48 %; purity, >95 %; m.p: 49–51 °C. ^{1}H NMR (400 MHz, $CDCl_3$) δ 7.82 (d, *J* = 7.9 Hz, 1H, H_6 coumarin ring), 7.58 (t, *J* = 7.8 Hz, 1H, H_8 coumarin ring), 7.36-7.27 (m, 2H, H_7, H_9 coumarin ring), 5.71 (s, 1H, H_3 coumarin ring), 4.29 (t, *J* = 5.4 Hz, 2H, –OCH_2-), 3.65 (t, *J* = 5.2 Hz, 2H, –CH_2O-), 2.97 (t, *J* = 5.4 Hz, 2H, –OCH_2-), 2.68-2.48 (m, 10H, -N-CH_2 × 4 piperazine ring, -N-CH_2). ^{13}C NMR (100 MHz, $CDCl_3$) δ 165.5 (C_4 coumarin ring), 162.8 (C_2 coumarin ring), 153.3 (C_{10} coumarin ring), 132.5 (C_8 coumarin ring), 124.0 (C_7 coumarin ring), 123.0 (C_6 coumarin ring), 116.8 (C_9 coumarin ring), 115.6 (C_5 coumarin ring), 90.7 (C_3 coumarin ring), 67.7 (-O-C-), 59.3 (-C-O-), 57.6 (-O-C-), 56.2 (-C-N-), 53.1 × 2 (-C-N × 2 piperazine ring), 52.9 × 2 (-N-C × 2 piperazine ring). LC-MS *m/z*: 341.2 [M + Na] $^+$.

4.4.10. 4-(3-(4-Ethylpiperazin-1-yl)propoxy)-2H-1-benzopyran-2-one (C1)

White solid; yield: 50 %; purity, >95 %; m.p: 80–82 °C. ^{1}H NMR (400 MHz, $CDCl_3$) δ 7.81 (d, *J* = 7.9 Hz, 1H, H_6 coumarin ring), 7.55 (t, *J* = 7.8 Hz, 1H, H_8 coumarin ring), 7.34-7.27 (m, 2H, H_7, H_9 coumarin ring), 5.71 (s, 1H, H_3 coumarin ring), 4.21 (t, *J* = 6.3 Hz, 2H, –OCH_2-), 2.65-2.40 (m, 12H, -N-CH_2 × 4 piperazine ring, -N-CH_2 × 2), 2.17-2.05 (m, 2H, –CH_2-), 1.11 (t, *J* = 7.2 Hz, 3H, –CH_3). ^{13}C NMR (100 MHz, $CDCl_3$) δ 165.7 (C_4 coumarin ring), 163.0 (C_2 coumarin ring), 153.3 (C_{10} coumarin ring), 132.4 (C_8 coumarin ring), 123.9 (C_7 coumarin ring), 123.0 (C_6 coumarin ring), 116.8 (C_9 coumarin ring), 115.8 (C_5 coumarin ring), 90.5 (C_3 coumarin ring), 67.6 (-O-C-), 54.7 (-C-N-), 53.1 × 2 (-C-N × 2 piperazine ring), 52.7 × 2 (-N-C × 2 piperazine ring), 52.3 (-N-C-), 26.0 (-C-C-), 11.8 (-CH_3). LC-MS *m/z*: 317.2 [M + H] $^+$.

4.4.11. 4-(3-(4-(2-Methoxyethyl)piperazin-1-yl)propoxy)-2H-1-benzopyran-2-one (C2)

White solid; yield: 49 %; purity, >95 %; m.p: 68–70 °C. ^{1}H NMR (400 MHz, $CDCl_3$) δ 7.81 (d, *J* = 7.9 Hz, 1H, H_6 coumarin ring), 7.55 (t, *J* = 7.8 Hz, 1H, H_8 coumarin ring), 7.33-7.25 (m, 2H, H_7, H_9 coumarin ring), 5.70 (s, 1H, H_3 coumarin ring), 4.20 (t, *J* = 6.2 Hz, 2H, –OCH_2-), 3.53 (t, *J* = 5.6 Hz, 2H, –CH_2O-), 3.35 (s, 3H, –OCH_3), 2.72-2.42 (m, 12H, -N-CH_2 × 4 piperazine ring, -N-CH_2 × 2), 2.14-2.06 (m, 2H, –CH_2-). ^{13}C NMR (100 MHz, $CDCl_3$) δ 165.7 (C_4 coumarin ring), 163.0 (C_2 coumarin ring), 153.3 (C_{10} coumarin ring), 132.4 (C_8 coumarin ring), 123.9 (C_7 coumarin ring), 123.0 (C_6 coumarin ring), 116.8 (C_9 coumarin ring), 115.8 (C_5 coumarin ring), 90.5 (C_3 coumarin ring), 70.0 (-C-O-), 67.6 (-O-C-), 58.9(-O-CH_3), 57.8 (-C-N-), 54.6 (-N-C-), 53.4 × 2 (-C-N × 2 piperazine ring), 52.9 × 2 (-N-C × 2 piperazine ring), 26.0 (-C-C-). LC-MS *m/z*: 347.2 [M + H] $^+$.

4.4.12. 4-(3-((3-Morpho-linopropyl)amino)propoxy)-2H-1-benzopyran-2-one (C3)

White solid; yield: 48 %; purity, >95 %; m.p: 58–59 °C. ^{1}H NMR (400 MHz, $CDCl_3$) δ 7.89 (d, *J* = 7.9 Hz, 1H, H_6 coumarin ring), 7.62 (t, *J* = 7.8 Hz, 1H, H_8 coumarin ring), 7.36-7.28 (m, 2H, H_7, H_9 coumarin ring), 5.82 (s, 1H, H_3 coumarin ring), 4.34 (t, *J* = 5.9 Hz, 2H, –OCH_2-), 3.73-3.66 (m, 4H, –CH_2O × 2 morpholine ring), 3.26-3.16 (m, 2H, –CH_2-N-), 3.08 (t, *J* = 7.3 Hz, 2H, -N-CH_2-), 2.55-2.45 (m, 6H, –NCH_2 × 2, -N-CH_2-), 2.37-2.26 (m, 2H, –CH_2-), 1.95-1.85 (m, 2H -CH_2-). ^{13}C NMR (100 MHz, $CDCl_3$) δ 165.3 (C_4 coumarin ring), 163.0 (C_2 coumarin ring), 152.5 (C_{10} coumarin ring), 132.0 (C_8 coumarin ring), 123.5 (C_7 coumarin ring), 122.2 (C_6 coumarin ring), 115.6 (C_9 coumarin ring), 114.7 (C_5 coumarin ring), 89.4 (C_3 coumarin ring), 66.2 (-O-C-), 65.8 × 2 (-C-O × 2 morpholine ring), 55.3 (-C-N), 52.6 × 2 (-N-C × 2 morpholine ring), 46.4 (-C-N-), 44.4 (-N-C-), 25.5 (-C-C-), 22.4 (-C-C-). LC-MS *m/z*: 347.2 [M + H] $^+$.

4.4.13. 4-(3-(4-(2-Hydroxyethyl)piperazin-1-yl)propoxy)-2H-chromen-2-one (C4)

White solid; yield: 48 %; purity, >95 %; m.p: 65–68 °C. ^{1}H NMR (400 MHz, $CDCl_3$) δ 7.71 (d, *J* = 7.9 Hz, 1H, H_6 coumarin ring), 7.45 (t, *J* = 7.8 Hz, 1H, H_8 coumarin ring), 7.25-7.15 (m, 2H, H_7, H_9 coumarin ring), 5.61 (s, 1H, H_3 coumarin ring), 4.11 (t, *J* = 6.3 Hz, 2H, –OCH_2-), 3.53 (t, *J* = 5.4 Hz, 2H, –CH_2O-), 2.55-2.40 (m, 12H, -N-CH_2 × 4 piperazine ring, -N-CH_2 × 2), 2.05-1.95 (m, 2H, –CH_2-). ^{13}C NMR (100 MHz, $CDCl_3$) δ 165.5 (C_4 coumarin ring), 162.9 (C_2 coumarin ring), 153.3 (C_{10} coumarin ring), 132.4 (C_8 coumarin ring), 123.9 (C_7 coumarin ring), 123.1 (C_6 coumarin ring), 116.8 (C_9 coumarin ring), 115.7 (C_5 coumarin ring), 90.7 (C_3 coumarin ring), 67.6 (-O-C-), 56.22 (-C-N-), 53.5 × 2 (-C-N × 2 piperazine ring), 53.2 × 2 (-N-C × 2 piperazine ring), 38.4 (-N-C-), 5.73 (-C-C-). LC-MS *m/z*: 355.1 [M + Na] $^+$.

4.4.14. 4-(3-((2-(Thiophen-2-yl)ethyl)amino)propoxy)-2H-1-benzopyran-2-one (C5)

Yellow oily; yield: 43 %; purity, >95 %. ^{1}H NMR (400 MHz, $CDCl_3$) δ 7.80 (d, *J* = 7.8 Hz, 1H, H_6 coumarin ring), 7.55 (t, *J* = 7.8 Hz, 1H, H_8 coumarin ring), 7.36-7.26 (m, 2H, H_7, H_9 coumarin ring), 7.13 (d, *J* = 5.1 Hz, 1H, -S-CH- thiophene ring), 6.95-6.89 (m, 1H, -CH- thiophene ring), 6.84 (d, *J* = 3.3 Hz, 1H, -CH- thiophene ring), 5.69 (s, 1H, H_3 coumarin ring), 4.22 (t, *J* = 6.1 Hz, 2H, –OCH_2-), 3.07 (t, *J* = 6.6 Hz, 2H, -N-CH_2), 3.01-2.95 (m, 2H, -N-CH_2), 2.94-2.87 (m, 2H, –CH_2-), 2.15-2.07 (m, 2H, –CH_2-). ^{13}C NMR (100 MHz, $CDCl_3$) δ 165.7 (C_4 coumarin ring), 163.0 (C_2 coumarin ring), 153.3 (C_{10} coumarin ring), 142.2 (-S-C- thiophene ring), 132.4 (C_8 coumarin ring), 126.9 (-S-CH- thiophene ring), 125.2 (-C-C- thiophene ring), 123.9 (C_7 coumarin ring), 123.7 (-C-C- thiophene ring), 123.0 (C_6 coumarin ring), 116.8 (C_9 coumarin ring), 115.7 (C_5 coumarin ring), 90.6 (C_3 coumarin ring), 67.5 (-O-C-), 50.9 (-C-N-), 46.0 (-N-C-), 30.2 (-C-C-), 28.8 (-C-C-). LC-MS *m/z*: 352.1 [M + Na] $^+$.

4.4.15. 4-(3-(3-Methylpiperidin-1-yl)propoxy)-2H-1-benzopyran-2-one (C6)

Yellow solid; yield: 48 %; purity, >95 %. ^{1}H NMR (400 MHz, $CDCl_3$) δ 7.84 (d, J = 7.9 Hz, 1H, H_6 coumarin ring), 7.57 (t, J = 7.8 Hz, 1H, H_8 coumarin ring), 7.36-7.29 (m, 2H, H_7, H_9 coumarin ring), 5.72 (s, 1H, H_3 coumarin ring), 4.23 (t, J = 6.2 Hz, 2H, –OCH_2-), 3.01-2.91 (m, 2H, -N-CH_2-), 2.63-2.59 (m, 2H, -N-CH_2-), 2.24-2.10 (m, 2H, -N-CH_2-), 1.98-1.95 (m, 2H, –CH_2-), 1.85-1.59 (m, 5H, –CH_2 × 2 piperidine ring, -CH- piperidine ring), 0.91 (d, J = 6.2 Hz, 3H, –CH_3). ^{13}C NMR (100 MHz, $CDCl_3$) δ 165.3 (C_4 coumarin ring), 162.6 (C_2 coumarin ring), 152.9 (C_{10} coumarin ring), 132.0 (C_8 coumarin ring), 123.5 (C_7 coumarin ring), 122.6 (C_6 coumarin ring), 116.4 (C_9 coumarin ring), 115.4 (C_5 coumarin ring), 90.1 (C_3 coumarin ring), 67.5 (-O-C-), 61.7 (-N-C- piperidine ring), 54.8 (-C-N-), 53.7 (-N-C- piperidine ring), 32.5 (-C-C- piperidine ring), 30.7 (-C-C-), 25.7 (-C-C- piperidine ring), 25.0 (-C-C- piperidine ring), 19.4 (-CH_3). LC-MS m/z: 302.2 [M + H] $^+$.

4.4.16. 4-(3-((3-(Pyrrolidin-1-yl)propyl)amino)propoxy)-2H-1-benzopyran-2-one (C7)

Yellow oily; purity, >95 %; yield: 43 %. ^{1}H NMR (400 MHz, $CDCl_3$) δ 7.84 (d, J = 7.9 Hz, 1H, H_6 coumarin ring), 7.58 (t, J = 7.8 Hz, 1H, H_8 coumarin ring), 7.37-7.30 (m, 2H, H_7, H_9 coumarin ring), 5.73 (s, 1H, H_3 coumarin ring), 4.26 (t, J = 6.0 Hz, 2H, –OCH_2-), 2.89 (t, J = 6.9 Hz, 2H, –CH_2-N-), 2.76 (t, J = 6.8 Hz, 2H, –CH_2-N-), 2.64-2.58 (m, 6H, –CH_2-N × 3), 2.17-2.08 (m, 2H, –CH_2-), 1.86-1.78 (m, 6H, –CH_2 × 2 pyrrolidine ring, –CH_2-). ^{13}C NMR (100 MHz, $CDCl_3$) δ 165.7 (C_4 coumarin ring), 163.0 (C_2 coumarin ring), 153.4 (C_{10} coumarin ring), 132.4 (C_8 coumarin ring), 123.9 (C_7 coumarin ring), 123.0 (C_6 coumarin ring), 116.8 (C_9 coumarin ring), 115.8 (C_5 coumarin ring), 90.6 (C_3 coumarin ring), 67.6 (-O-C-), 54.7 (-C-N-), 54.2 × 2 (-N-C × 2 pyrrolidine ring), 48.5 (-C-N-), 46.3 (-N-C-), 29.0 (-C-C-), 28.7 (-C-C-), 23.4 × 2 (-C-C × 2 pyrrolidine ring). LC-MS m/z: 331.2 [M + Na] $^+$.

4.4.17. 4-(3-(4-Acetylpiperazin-1-yl)propoxy)-2H-chromen-2-one (C8)

Yellowish solid; yield: 43 %; purity, >95 %; m.p: 125–126 °C. ^{1}H NMR (400 MHz, DMSO) δ 7.84 (d, J = 7.4 Hz, 1H, H_6 coumarin ring), 7.68 (t, J = 7.7 Hz, 1H, H_8 coumarin ring), 7.43-7.37 (m, 2H, H_7, H_9 coumarin ring), 5.92 (s, 1H, H_3 coumarin ring), 4.28 (t, J = 6.0 Hz, 2H, –OCH_2-), 3.47-3.40 (m, 4H, –CH_2-N- hydrogen on piperazine near carbonyl group), 2.55-2.49 (m, 4H, –CH_2-N × 2 hydrogen on the Piperidine away from the carbonyl group), 2.42 (t, J = 5.2Hz, 2H, –NCH_2-), 2.35 (t, J = 5.2Hz, 2H, –CH_2-), 2.00 (s, 3H, –CH_3). ^{13}C NMR (100 MHz, $CDCl_3$) δ 168.9 (-C=O), 165.6 (C_4 coumarin ring), 162.9 (C_2 coumarin ring), 153.4 (C_{10} coumarin ring), 132.5 (C_8 coumarin ring), 123.9 (C_7 coumarin ring), 122.9 (C_6 coumarin ring), 116.8 (C_9 coumarin ring), 115.7 (C_5 coumarin ring), 90.6 (C_3 coumarin ring), 67.4 (-O-C-), 54.5 (-C-N-), 53.5 (-C-N- carbon on piperazine near carbonyl group), 52.8 (-C-N- carbon on piperazine near carbonyl group), 46.2 (-C-N- carbon on the piperidine away from the carbonyl group), 41.3 (-C-N- carbon on the piperidine away from the carbonyl group), 25.9 (-C-C-), 21.4 (-CH_3). LC-MS m/z: 331.2 [M + Na] $^+$.

4.5. Cell lines and biological reagents

J774A.1 cells were purchased from ATCC (Manassas, VA) and cultured in DMEM medium (Invitrogen, Carlsbad, CA) enriched with 10 % fetal bovine serum (FBS), 1 % penicillin and 1 % streptomycin, and placed in a 37 °C incubator. LPS was purchased from Sigma-Aldrich (St Louis, MO, USA). Mouse IL-6 Kit was bought from eBioscience Inc (San Diego, CA, USA). Anti- GAPDH, anti-IκB-α, anti-p65, anti-p-p65 and anti-p38, anti-p-p38, anti-JNK and anti-P-JNK were bought from Cell Signaling Technology (Danvers, MA, USA). Trizol reagent and Real-time quantitative reverse transcription PCR (RT-qPCR) kit were purchased from TaKaRa (Japan). The cDNA kit was bought from Yeasen Biotechnology (Shanghai, China).

4.6. Detection of the expression level of IL-6

When the J774A.1 cells adhered to the 96-well plate, the prepared drug was added to the hole, and the final concentration of the drug was 10 μM. Afterincubation for 30 min, LPS was added to each well, maintaining a concentration of 0.5 μg/mL for 24 h. The expression level of IL-6 was detected by commercial ELISA kit (BioScience, San Diego, CA). Subsequently, the remaining volume of 10 % MTT was added to the remaining medium of the 96-well plate hole to detect the OD value. The total concentration of inflammatory factors in the medium was normalized by the number of living cells.

4.7. MTT assay

In each well of a 96-well plate, 100 μL of cell suspension containing 8000 cells/mL was dispensed. Following placement in a temperature-controlled incubator for 24 h, the designated compounds were introduced to the wells at a final concentration of 10 μM. Subsequently, the cell viability was assessed after a 24-h incubation period. Cells in each well were incubated with 10 % MTT solution (5.0 mg/mL) for 4 h. Next, the medium was aspirated using a syringe and discarded. Subsequently, 150 μL of DMSO was added to each well and shaken for 30 min. At the wavelength of 490 nm, the OD value was detected.

4.8. Real-time quantitative reverse transcription PCR assay

Total RNA was extracted from cells using triazole (TaKaRa, Japan). Total RNA concentration and purity were measured using a UV–visible spectrophotometer NanoDrop 2000 (Thermo Science, USA). The RNA was reverse-transcribed into cDNA using a cDNA kit (Yeasen Biotechnology, Shanghai), and then RT-qPCR was performed using a RT-qPCR kit (TaKaRa, Japan) and a LightCycler® 480 instrument (Roche, Switzerland). The mRNA level of the target gene was normalized with the expression level of the β-actin as the reference gene.

4.9. Western blotting

J774A.1 macrophages were pre-treated with **B8** at concentrations of 20, 10, and 5 μM for 2 h, followed by stimulation with lipopolysaccharide (0.5 μg/mL) for 30 min. Subsequently, the cells were lysed on ice using RIPA buffer to extract total protein, which was quantified using the Bradford colorimetric method. The protein samples were diluted to a concentration of 2 μg/μL using a loading buffer, heated at 100 °C for 5 min. Subsequently, 40 μg of each sample was loaded onto a 12.5 % sodium dodecyl sulfate-polyacrylamide gel electrophoresis (SDS-PAGE) and transferred onto a polyvinylidene fluoride (PVDF) membrane. The PVDF membrane was blocked with bovine serum albumin for 1.5 h, and then incubated with the primary antibody at 4 °C overnight. This was followed by incubation with secondary antibody at room temperature for 2 h. Finally, the blots were detected by an ECL detection reagent.

4.10. Acute toxicity test

The ICR mice (n = 24, 8 weeks, male, weight: 30 g ± 2 g) were purchased from the Experimental Animal Center of Zhejiang Province. The mice were randomly divided into three groups, **B8**-1000 mg/kg, **B8**-500 mg/kg, and normal control group. After 1 week of adaptation, the mice were gavaged. Different concentrations of compound **B8** were dissolved in 0.5 % DMSO and subsequently added into normal saline to prepare a solution. The mice were gavaged daily; their body weight and behavior were recorded and monitored daily. After 10 days, the mice were euthanized by intraperitoneal injection of excessive anesthetics. The important organs of mice, such as heart, liver, spleen, lung and kidney, were taken and stained to observe the histomorphological changes.

4.11. Pharmacokinetic analysis of compound **B8**

Male SD rats (n = 6, 8 weeks, body weight 200 g ± 20 g) were obtained from Zhejiang Experimental Animal Center. They were randomly divided into two groups: three to receive oral administration and three to receive tail vein injection of the drugs. Rats were intragastrically administered with a dose of 10 mg/kg **B8** dissolved in 0.05 % DMSO and normal saline. The volume was adjusted according to the rats' body weight. Blood samples were collected from the tail vein at 10 min, 15 min, 30 min, 1 h, 2 h, 3 h, 4 h, 5 h, 6 h, 8 h, 10 h, 12 h, and 24 h after administration. A dose of 1 mg/kg was administered via tail vein. **B8** was dissolved in 5 % DMSO, mixed with 30 % PEG400 and 65 % normal saline. The mixture was administered to the rats at a volume based on the weight. At 5 min, 10 min, 15 min, 30 min, 1 h, 2 h, 3 h, 4 h, 5 h, 6 h, 8 h, 10 h, 12 h, 24 h, blood samples were collected from the tail vein and transferred into 1.5 mL heparin sodium tube. All blood samples were centrifuged at 8000 rpm for 15 min, and 200 μL of supernatant was transferred into a new 1.5 mL tube. Next, 40 μL of supernatant was added to a new 1.5 mL tube with 0.2 mL of acetonitrile precipitation solution containing internal standard, vortexed for 2 min, and centrifuged at 12000 rpm for 15 min. The supernatant was collected and analyzed by triple quadrupole mass spectrometer (H-CLASS + XEVO TQS-MICRO).

4.12. DSS-induced mouse IBD model and compounds treatment

Male 8-weeks-old mice (C57BL/6) weighing approximately 22 g were procured from Zhejiang Experimental Animal Center in Hangzhou, China. Before experiments, the mice were allowed to acclimatize to the laboratory environment in a room with a constant temperature of 22 ± 2 °C, humidity of 55 ± 5 %, and a light-dark cycle of 12 h for 5 days. They were allowed free access to water and food. All animal experiments were conducted in accordance with the guidelines of the National Institutes of Health Guide and Care of Laboratory Animals. This study was approved by the Animal Protection and Utilization Committee of Wenzhou Medical University. A total of 30 mice were randomly assigned into five groups, with six mice in each group. These groups included a control group, a model group, a 4-HC group, a compound **B8** group, and a 5-ASA group. To establish an IBD model, mice in the model group, 4-HC group, optimal compound **B8** group, and 5-ASA group were administered with 2.5 % DSS in their drinking water for seven days, while those in the control group was given distilled water for 10 days. These mice experiments were approved by the Animal Protection and Utilization Committee of Wenzhou Medical University. Mice were categorized into five groups, each with 6 mice: control group, model group, 4-HC group, compound **B8** group, and 5-ASA group. To establish an IBD model, mice in the model group, 4-HC group, optimal compound **B8** group, and 5-ASA group were administered with 2.5 % DSS in their drinking water for 7 days, while those in the control group was provided with distilled water for 10 days. The drinking water was changed every two days. Compound **B8** and 4-HC were orally administered at a dose of 20 mg/kg (po, qd) for 7 consecutive days, while 5-ASA was orally administered at a dose of 100 mg/kg (po, qd) for the same duration. On the eighth day, the DSS was replaced with distilled water, which was intragastrically administered for 3 days. All compounds that were intragastrically administered were dissolved in 5 % DMSO and added to a 95 % solution containing 5 % CMC-Na. In addition, mice in the control and model groups were gavaged with excipients. Changes in mouse weight, stool consistency, rectal bleeding, and other indicators were recorded. After anesthetization, blood was collected from the eyeball and the mice were sacrificed. The colon was removed and its length was measured. The concentration of inflammatory factors in the blood was determined. Colon tissues were collected immediately, fixed with 4 % formaldehyde, and stored for subsequent H&E staining analysis and immunohistochemistry. The remaining colon tissues were stored at −80 °C for further experiments.

4.13. The severity of IBD was assessed according to the disease activity index

Disease activity index (DAI) is often used as an indicator for assessing the severity of IBD. Briefly, the pathological features of each mouse were scored daily, including the consistency of stool, whether there was bloody stool, and weight loss. The scores of each mouse were combined and averaged to obtain DAI. The scores ranged from 0 to 4, the highest being 4 points (Table S1).

4.14. Animal model of ALI

Mice (n = 24, C57BL/6, 20 ± 2 g) were purchased from Vital River, Zhejiang. They were used for experiments after one week of adaptation to the laboratory conditions. The mice were randomly divided into 4 groups with 6 mice in each group: control group, LPS group, dexamethasone group and **B8** group. The control group and the LPS group were given an equal volume of 0.9 % normal saline, and the dexamethasone group and the **B8** group were given 20 mg/kg by gavage three times at an interval of 12 h. After the last gavage, the mice were anesthetized and sham-operated in the control group. The mice in the LPS group, dexamethasone group and **B8** group were intratracheally injected with LPS at a dose of 5 mg/kg. After 6 h of stimulation, an appropriate amount of anesthetic was injected intraperitoneally and blood was collected. The supernatant was collected after centrifugation and the level of IL-6 was measured. The left lung was rinsed with 3 × 200 μL normal saline, and the lavage fluid was collected and centrifuged to obtain alveolar lavage fluid. The inflammatory factors, total protein content and neutrophil count in BALF were measured. The lung tissues were collected for H&E staining and immunohistochemistry. Finally, the rat bodies were cremated.

4.15. Pathological examination of lung, Intestine and spleen in mice

To prepare paraffin-embedded tissue sections, lung tissue, spleen, and intestinal tissue were collected and fixed with 4 % paraformaldehyde (PFA). Subsequently, the tissues were processed and embedded in paraffin. The resulting paraffin block, containing the sample, was then sectioned into thin slices with a thickness of 5 μm. These sections are subsequently stained with Hematoxylin and Eosin (H&E staining kit, Beyotime, Shanghai, China) for further examination.

To perform immunohistochemical analyses on intestinal and lung sections, tissue samples were subjected to dehydrocarbonization with xylene and then rehydrated through a series of graded ethanol solutions. Antigen recovery was achieved by boiling the sections in sodium citrate buffer (pH = 6) for 25 min. Subsequently, the sections were incubated with specific primary antibody at 4 °C for 12 h, followed by incubation with the secondary antibody (1: 2000; santa Cruz, United States). The sections were treated with 3,3-diaminobenzidine (DAB) (ZSGB-Bio, Beijing, China), stained with hematoxylin, and observed under a microscope (Carl Zeiss).

4.16. Molecular docking

The crystal structures of IRAK1 (PDB: 6BFN), MD2 (PDB: 2E56), TAK1 (PDB: 7NTH), TLR4 (PDB: 7MLM), p38 (PDB: 6OHD), IKKβ (PDB: 3RZF), JNK (PDB: 1PMV), IRAK4 (PDB: 6RFJ), ERK2 (PDB: 1TVO), IKK1 (PDB: 5TQW), TAB2 (PDB: 2WWZ) were extracted from the protein database. TRAF6 (PDB: 1LB4), p65 (PDB: 1IKN), Myd88 (PDB: 7BER). The three-dimensional structure of compound **B8** minimizes the energy of MM2 by using Chem Draw 16.0. Maestro software was used to optimize the compounds and proteins. The docking box is generated based on the original ligand in the protein crystal structure. Maestro software was used for docking scoring. Then the results of the docking are imported into Pymol for drawing.

4.17. Statistical analysis

Data from different groups were analyzed using Student 's *t*-test multiple comparisons in GraphPad Prism 9.0 (GraphPad, San Diego, CA). The results were expressed as mean ± standard error of three independent experiments. $P < 0.05$ was considered statistically significant.

CRediT authorship contribution statement

Xiaobo Li: Writing – review & editing, Writing – original draft, Methodology, Investigation, Formal analysis, Data curation, Conceptualization. **Xinyi Huang:** Supervision, Software. **Yunxi Zhao:** Formal analysis, Data curation. **Zhiwei Zheng:** Validation, Conceptualization. **Mi Guo:** Resources, Methodology, Investigation. **Zhicao Chen:** Validation. **Pan Chen:** Visualization, Validation, Supervision. **Xiang Li:** Formal analysis. **Jing Liao:** Validation. **Miao Jiang:** Investigation. **Won-Jea Cho:** Conceptualization. **Young-Chang Cho:** Conceptualization. **Ruifeng Zeng:** Resources, Conceptualization. **Qidong Tang:** Writing – review & editing, Conceptualization. **Guang Liang:** Supervision, Funding acquisition, Conceptualization.

Declaration of competing interest

The authors declare that they have no known competing financial interests or personal relationships that could have appeared to influence the work reported in this paper.

Data availability

Data will be made available on request.

Acknowledgments

This study was financially supported by the National Natural Science Funding of China (82273791), Zhejiang Provincial Key Scientific Project (2021C03041), Scientific Research Starting Foundation in Wenzhou Medical University (QTJ21013), Basic Public Welfare Research Project of Wenzhou City (Y20220945), Research Fund from the University of Chinese Academy of Sciences (WIUCASQD2020016), and Basic Public Welfare Research Project of Zhejiang Province (LGD20H090003). We thank Scientific Research Center of Wenzhou Medical University for consultation and instrument availability that supported this work.

Appendix A. Supplementary data

Supplementary data to this article can be found online at https://doi.org/10.1016/j.ejmech.2024.116487.

References

[1] S. Miranda-Castro, F.J. Aidar, S.S. de Moura, L. Marcucci-Barbosa, L.F. Lobo, F. de Assis Dias Martins-Junior, R. da Silva Filha, P.A.S. Vaz de Castro, E.S.A.C. Simoes, D. da Gloria de Souza, S.A. da Silva, K.M. de Castro Pinto, G. de Paula Costa, A. F. Silva, F.M. Clemente, W.V.C. Pereira, A. Nunes-Silva, The curcumin supplementation with piperine can influence the acute elevation of exercise-induced cytokines: double-blind crossover study, Biology 11 (2022).

[2] J. Garcia Diaz, R. Gonzalez Fernandez, J.C. Escalona Arranz, G. Llaurado Maury, D. Mendez Rodriguez, L. De Vooght, E. Molina, E. Tuenter, L. Pieters, P. Cos, Inhibitory effect on nitric oxide release in LPS-stimulated macrophages and free radical scavenging activity of Croton linearis jacq. Leaves, Antioxidants 11 (2022).

[3] A. Weidinger, L. Birgisdottir, J. Schaffer, A.T. Meszaros, S. Zavadskis, A. Mullebner, M. Hecker, J.C. Duvigneau, N. Sommer, A.V. Kozlov, Systemic effects of mitoTEMPO upon lipopolysaccharide challenge are due to its antioxidant part, while local effects in the lung are due to triphenylphosphonium, Antioxidants 11 (2022).

[4] M. Sasai, M. Yamamoto, Pathogen recognition receptors: ligands and signaling pathways by Toll-like receptors, Int. Rev. Immunol. 32 (2013) 116–133.

[5] J. Dudeck, A. Medyukhina, J. Frobel, C.M. Svensson, J. Kotrba, M. Gerlach, A. C. Gradtke, B. Schroder, S. Speier, M.T. Figge, A. Dudeck, Mast cells acquire MHCII from dendritic cells during skin inflammation, J. Exp. Med. 214 (2017) 3791–3811.

[6] Y. Zhang, X. He, X. Wu, M. Lei, Z. Wei, X. Zhang, L. Wen, P. Xu, S. Li, S. Qu, Rapamycin upregulates glutamate transporter and IL-6 expression in astrocytes in a mouse model of Parkinson's disease, Cell Death Dis. 8 (2017) e2611.

[7] W. Ko, N. Kim, H. Lee, E.R. Woo, Y.C. Kim, H. Oh, D.S. Lee, Anti-inflammatory effects of compounds from cudrania tricuspidata in HaCaT human keratinocytes, Int. J. Mol. Sci. 22 (2021).

[8] J. Zeng, N. Zhao, J. Yang, W. Kuang, X. Xia, X. Chen, Z. Liu, R. Huang, Puerarin induces molecular details of ferroptosis-associated anti-inflammatory on RAW264.7 macrophages, Metabolites 12 (2022).

[9] A. Seliga, M.H. Lee, N.C. Fernandes, V. Zuluaga-Ramirez, M. Didukh, Y. Persidsky, R. Potula, S. Gallucci, U. Sriram, Kallikrein-kinin system suppresses type I interferon responses: a novel pathway of interferon regulation, Front. Immunol. 9 (2018) 156.

[10] B. Yang, Z. Gao, Q.S. Li, X.Y. Zhang, L. Song, Y.N. Wang, X.Y. Wang, L.L. Ji, H. L. Xu, H. Xie, F.K. Feng, X.P. Li, W. Li, R. Wang, G.S. Wang, Proteomic analysis and identification reveal the anti-inflammatory mechanism of clofazimine on lipopolysaccharide-induced acute lung injury in mice, Inflamm. Res. 71 (2022) 1327–1345.

[11] J. Zhang, Q. Li, X. Zhang, Y. Chen, Y. Lu, X. Wang, L. Zhang, T. Wang, Bisdemethoxycurcumin alleviates dextran sodium sulfate-induced colitis via inhibiting NLRP3 inflammasome activation and modulating the gut microbiota in mice, Antioxidants 11 (2022).

[12] H. Lee, M. Krishnan, M. Kim, Y.K. Yoon, Y. Kim, Rhamnetin, a natural flavonoid, ameliorates organ damage in a mouse model of carbapenem-resistant acinetobacter baumannii-induced sepsis, Int. J. Mol. Sci. 23 (2022).

[13] J. Sommer, E. Engelowski, P. Baran, C. Garbers, D.M. Floss, J. Scheller, Interleukin-6, but not the interleukin-6 receptor plays a role in recovery from dextran sodium sulfate-induced colitis, Int. J. Mol. Med. 34 (2014) 651–660.

[14] S.H. Mei, S.D. McCarter, Y. Deng, C.H. Parker, W.C. Liles, D.J. Stewart, Prevention of LPS-induced acute lung injury in mice by mesenchymal stem cells overexpressing angiopoietin 1, PLoS Med. 4 (2007) e269.

[15] F. Xu, J. Gao, S. Bergmann, A.C. Sims, D.G. Ashbrook, R.S. Baric, Y. Cui, C. B. Jonsson, K. Li, R.W. Williams, K. Schughart, L. Lu, Genetic dissection of the regulatory mechanisms of Ace2 in the infected mouse lung, Front. Immunol. 11 (2020) 607314.

[16] Y. Zhang, D. Liang, L. Dong, X. Ge, F. Xu, W. Chen, Y. Dai, H. Li, P. Zou, S. Yang, G. Liang, Anti-inflammatory effects of novel curcumin analogs in experimental acute lung injury, Respir. Res. 16 (2015) 43.

[17] T. Yamane, K. Uchiyama, T. Ishii, H. Ishii, M. Omura, K. Fujise, H. Tajiri, Refractory diverticular colitis with progressive ulcerative colitis-like changes extending to the rectum, Dig. Endosc. 21 (2009) 188–191.

[18] M. Gao, C. Yang, C. Wu, Y. Chen, H. Zhuang, J. Wang, Z. Cao, Hydrogel-metal-organic-framework hybrids mediated efficient oral delivery of siRNA for the treatment of ulcerative colitis, J. Nanobiotechnol. 20 (2022) 404.

[19] A.L. Matthis, B. Zhang, L.A. Denson, B.R. Yacyshyn, E. Aihara, M.H. Montrose, Importance of the evaluation of N-acetyltransferase Enzyme activity prior to 5-aminosalicylic acid medication for ulcerative colitis, Inflamm. Bowel Dis. 22 (2016) 1793–1802.

[20] Y. Liu, Y. Zhang, X. Zheng, T. Fang, X. Yang, X. Luo, A. Guo, K.A. Newell, X. F. Huang, Y. Yu, Galantamine improves cognition, hippocampal inflammation, and synaptic plasticity impairments induced by lipopolysaccharide in mice, J. Neuroinflammation 15 (2018) 112.

[21] A. Trifan, G. Zengin, K.I. Sinan, E. Sieniawska, R. Sawicki, M. Maciejewska-Turska, K. Skalikca-Wozniak, S.V. Luca, Unveiling the phytochemical profile and biological potential of five artemisia species, Antioxidants 11 (2022).

[22] E. Koziol, K. Jozwiak, B. Budzynska, P.A.M. de Witte, D. Copmans, K. Skalicka-Wozniak, Comparative antiseizure analysis of diverse natural coumarin derivatives in zebrafish, Int. J. Mol. Sci. 22 (2021).

[23] G. Chen, Y. Zhang, X. Liu, Q. Fang, Z. Wang, L. Fu, Z. Liu, Y. Wang, Y. Zhao, X. Li, G. Liang, Discovery of a new inhibitor of myeloid differentiation 2 from cinnamamide derivatives with anti-inflammatory activity in sepsis and acute lung injury, J. Med. Chem. 59 (2016) 2436–2451.

[24] X. Li, L. Yin, J. Liao, J. Yang, B. Cai, Y. Yu, S. Su, Z. Du, X. Li, Y. Zhou, P. Chen, W. J. Cho, N. Chattipakorn, A.V. Samorodov, V.N. Pavlov, F. Zhang, G. Liang, Q. Tang, Novel O-benzylcinnamic acid derivative L26 treats acute lung injury in mice by MD-2, Eur. J. Med. Chem. 252 (2023) 115289.

[25] D. Yu, M. Suzuki, L. Xie, S.L. Morris-Natschke, K.H. Lee, Recent progress in the development of coumarin derivatives as potent anti-HIV agents, Med. Res. Rev. 23 (2003) 322–345.

[26] X.Y. Song, Y.Y. Wang, S.F. Chu, J.F. Hu, P.F. Yang, W. Zuo, L.K. Song, S. Zhang, N. H. Chen, A new coumarin derivative, IMM-H004, attenuates okadaic acid-induced spatial memory impairment in rats, Acta Pharmacol. Sin. 37 (2016) 444–452.

[27] E. Okuyama, T. Hasegawa, T. Matsushita, H. Fujimoto, M. Ishibashi, M. Yamazaki, Analgesic components of saposhnikovia root (Saposhnikovia divaricata), Chem. Pharm. Bull. (Tokyo) 49 (2001) 154–160.

[28] J. Neyts, E. De Clercq, R. Singha, Y.H. Chang, A.R. Das, S.K. Chakraborty, S. C. Hong, S.C. Tsay, M.H. Hsu, J.R. Hwu, Structure-activity relationship of new anti-hepatitis C virus agents: heterobicycle-coumarin conjugates, J. Med. Chem. 52 (2009) 1486–1490.

[29] R.N. Gacche, D.S. Gond, N.A. Dhole, B.S. Dawane, Coumarin Schiff-bases: as antioxidant and possibly anti-inflammatory agents, J. Enzym. Inhib. Med. Chem. 21 (2006) 157–161.

[30] R.S. Keri, K.M. Hosamani, R.V. Shingalapur, M.H. Hugar, Analgesic, anti-pyretic and DNA cleavage studies of novel pyrimidine derivatives of coumarin moiety, Eur. J. Med. Chem. 45 (2010) 2597–2605.
[31] A.C. Luchini, P. Rodrigues-Orsi, S.H. Cestari, L.N. Seito, A. Witaicenis, C. H. Pellizzon, L.C. Di Stasi, Intestinal anti-inflammatory activity of coumarin and 4-hydroxycoumarin in the trinitrobenzenesulphonic acid model of rat colitis, Biol. Pharm. Bull. 31 (2008) 1343–1350.
[32] J.J. Zhu, J.G. Jiang, Pharmacological and nutritional effects of natural coumarins and their structure-activity relationships, Mol. Nutr. Food Res. 62 (2018) e1701073.
[33] H. Fang, J. Zhang, M. Ao, F. He, W. Chen, Y. Qian, Y. Zhang, Y. Xu, M. Fang, Synthesis and discovery of omega-3 polyunsaturated fatty acid- alkanolamine (PUFA-AA) derivatives as anti-inflammatory agents targeting Nur77, Bioorg. Chem. 105 (2020) 104456.
[34] P. Chen, Y. Zhou, X. Li, J. Yang, Z. Zheng, Y. Zou, X. Li, J. Liao, J. Dai, Y. Xu, L. Yin, G. Chen, J. Gu, Q. Ouyang, W.J. Cho, Q. Tang, G. Liang, Design, synthesis, and bioevaluation of novel MyD88 inhibitor c17 against acute lung injury derived from the virtual screen, J. Med. Chem. 66 (2023) 6938–6958.
[35] J. Yang, M. Wang, Y. Xu, J. Liao, X. Li, Y. Zhou, J. Dai, X. Li, P. Chen, G. Chen, W. J. Cho, N. Chattipakorn, A.V. Samorodov, V.N. Pavlov, Y. Wang, G. Liang, Q. Tang, Discovery of 4-oxo-N-phenyl-1,4-dihydroquinoline-3-carboxamide derivatives as novel anti-inflammatory agents for the treatment of acute lung injury and sepsis, Eur. J. Med. Chem. 249 (2023) 115144.
[36] Y. Wang, W. Luo, J. Han, Z.A. Khan, Q. Fang, Y. Jin, X. Chen, Y. Zhang, M. Wang, J. Qian, W. Huang, H. Lum, G. Wu, G. Liang, MD2 activation by direct AGE interaction drives inflammatory diabetic cardiomyopathy, Nat. Commun. 11 (2020) 2148.
[37] S. Park, H.J. Shin, M. Shah, H.Y. Cho, M.A. Anwar, A. Achek, H.K. Kwon, B. Lee, T. H. Yoo, S. Choi, TLR4/MD2 specific peptides stalled in vivo LPS-induced immune exacerbation, Biomaterials 126 (2017) 49–60.
[38] S. Guo, M. Nighot, R. Al-Sadi, T. Alhmoud, P. Nighot, T.Y. Ma, Lipopolysaccharide regulation of intestinal tight junction permeability is mediated by TLR4 signal transduction pathway activation of FAK and MyD88, J. Immunol. 195 (2015) 4999–5010.
[39] Y. Zhong, K. Bry, J.D. Roberts Jr., IL-1beta dysregulates cGMP signaling in the newborn lung, Am. J. Physiol. Lung Cell Mol. Physiol. 319 (2020) L21–L34.
[40] S.K. Ippagunta, J.A. Pollock, N. Sharma, W. Lin, T. Chen, K. Tawaratsumida, A. A. High, J. Min, Y. Chen, R.K. Guy, V. Redecke, J.A. Katzenellenbogen, H. Hacker, Identification of Toll-like receptor signaling inhibitors based on selective activation of hierarchically acting signaling proteins, Sci. Signal. 11 (2018).
[41] M. Landstrom, The TAK1-TRAF6 signalling pathway, Int. J. Biochem. Cell Biol. 42 (2010) 585–589.
[42] J. Lee, T. Nakagiri, T. Oto, M. Harada, E. Morii, Y. Shintani, M. Inoue, Y. Iwakura, S. Miyoshi, M. Okumura, T. Hirano, M. Murakami, IL-6 amplifier, NF-kappaB-triggered positive feedback for IL-6 signaling, in grafts is involved in allogeneic rejection responses, J. Immunol. 189 (2012) 1928–1936.
[43] J.D. Smith, J. Brawley, K.C. Bordenave, R.K. Olsen, A. Intasiri, C.R. Cremo, T. W. Bell, Isoform selectivities of novel 4-hydroxycoumarin imines as inhibitors of myosin II, Eur. J. Med. Chem. 247 (2023).
[44] T. Ma, X. Tian, B. Zhang, M. Li, Y. Wang, C. Yang, J. Wu, X. Wei, Q. Qu, Y. Yu, S. Long, J.W. Feng, C. Li, C. Zhang, C. Xie, Y. Wu, Z. Xu, J. Chen, Y. Yu, X. Huang, Y. He, L. Yao, L. Zhang, M. Zhu, W. Wang, Z.C. Wang, M. Zhang, Y. Bao, W. Jia, S. Y. Lin, Z. Ye, H.L. Piao, X. Deng, C.S. Zhang, S.C. Lin, Low-dose metformin targets the lysosomal AMPK pathway through PEN2, Nature 603 (2022) 159–165.
[45] J. Liao, J. Yang, X. Li, C. Hu, W. Zhu, Y. Zhou, Y. Zou, M. Guo, Z. Chen, X. Li, J. Dai, Y. Xu, Z. Zheng, P. Chen, W.J. Cho, G. Liang, Q. Tang, Discovery of the diphenyl 6-Oxo-1,6-dihydropyridazine-3-carboxylate/carboxamide analogue J27 for the treatment of acute lung injury and sepsis by targeting JNK2 and inhibiting the JNK2-NF-kappaB/MAPK pathway, J. Med. Chem. 66 (2023) 12304–12323.
[46] L. Zheng, Y.L. Zhang, Y.C. Dai, X. Chen, D.L. Chen, Y.T. Dai, Z.P. Tang, Jianpi Qingchang decoction alleviates ulcerative colitis by inhibiting nuclear factor-kappaB activation, World J. Gastroenterol. 23 (2017) 1180–1188.
[47] H. Hozumi, J. Russell, S. Vital, D.N. Granger, IL-6 mediates the intestinal microvascular thrombosis associated with experimental colitis, Inflamm. Bowel Dis. 22 (2016) 560–568.
[48] L. Shi, N. Dong, D. Ji, X. Huang, Z. Ying, X. Wang, C. Chen, Lipopolysaccharide-induced CCN1 production enhances interleukin-6 secretion in bronchial epithelial cells, Cell Biol. Toxicol. 34 (2018) 39–49.